

Flavor structure of the nucleon electromagnetic form factors and transverse charge densities in the chiral quark-soliton model

António Silva,^{1,2,*} Diana Urbano,^{1,2,†} and Hyun-Chul Kim^{3,4,‡}

¹*Faculdade de Engenharia, Universidade do Porto,
rua Dr. Roberto Frias, P-4200-465 Porto, Portugal*

²*Centro de Física Computacional (CFC), Departamento de Física,
Universidade de Coimbra, P-3004-516 Coimbra, Portugal*

³*Department of Physics, Inha University, Incheon 402-751, Korea*

⁴*School of Physics, Korea Institute for Advanced Study (KIAS), Seoul 130-722, Republic of Korea*
(Dated: April, 2013)

We investigate the flavor decomposition of the electromagnetic form factors of the nucleon, based on the chiral quark-soliton model with symmetry-conserving quantization. We consider the rotational $1/N_c$ and linear strange-quark mass (m_s) corrections. To extend the results to higher momentum transfer, we take into account the kinematical relativistic effects. We discuss the results of the flavor-decomposed electromagnetic form factors in comparison with the recent experimental data. In order to see the effects of the strange quark, we compare the SU(3) results with those of SU(2). We finally discuss the transverse charge densities for both unpolarized and polarized nucleons.

PACS numbers: 13.40.Gp, 14.20.Dh, 14.20.Jn, 14.65.Bt

Keywords: Nucleon electromagnetic form factors, charge radii, flavor decomposition of the electromagnetic form factors, transverse charge densities

arXiv:1305.6373v1 [hep-ph] 28 May 2013

* ajsilva@fe.up.pt

† urbano@fe.up.pt

‡ hchkim@inha.ac.kr

I. INTRODUCTION

Electromagnetic form factors (EMFFs) are the most fundamental observables that reveal the charge and magnetization structures of the nucleon. A series of recent measurements of the EMFFs has renewed the understanding of the internal structure of the nucleon and has posed fundamental questions about its nonperturbative nature. The results of the ratio of the proton EMFFs, $\mu_p G_E^p/G_M^p$ with the proton magnetic moment μ_p , obtained by measuring the transverse and longitudinal recoil proton polarizations [1–8], were found to decrease almost linearly as Q^2 increases for $Q^2 > 1 (\text{GeV}/c)^2$. These results were in conflict with most previous measurements of the proton EMFFs from unpolarized electron-proton cross sections based on the Rosenbluth separation method [9]. These new experimental results have triggered subsequent theoretical and experimental works (see, for example, recent reviews [10–14]). This discrepancy is partially explained by the effects of two-photon exchange, which affect unpolarized electron-proton scattering at higher Q^2 but have less influence on the polarization measurements [15–20]. Moreover, the new experimental results of the proton EMFFs in a wider range of Q^2 provided a whole new perspective on the internal quark-gluon structure of the nucleon. Perturbative quantum chromodynamics (pQCD) with factorization schemes [21] predicts the different scalings of the Dirac and Pauli FFs, F_1^p and F_2^p : F_1^p falls off as $1/Q^4$ while F_2^p decreases as $1/Q^6$, so that $Q^2 F_2^p/F_1^p$ becomes flat at large Q^2 . However, the experimental data show that the ratio $Q^2 F_2^p/F_1^p$ increases with Q^2 but $Q F_2^p/F_1^p$ becomes flat starting around 2 GeV^2 . A similar discrepancy between the experimental data and pQCD was also found in the $\gamma\gamma^* \rightarrow \pi$ transition form factor [22, 23] even for higher Q^2 . The neutron EMFFs were also measured by various experiments with higher precision [24–34].

Assuming isospin and charge symmetries, neglecting the strangeness in the nucleon, and using both the experimental data for the proton and neutron EMFFs, Cates *et al.* [35] have extracted the up and down EMFFs and have obtained remarkable results: the Q^2 dependence of the up- and down-quark Dirac and Pauli form factors (FFs) are considerably different from each other. The down-quark Dirac and Pauli FFs are roughly proportional to $1/Q^4$ but those of the up-quark fall off more gradually. Moreover, while the ratios $\kappa_u^{-1} F_2^u/F_1^u$ and $\kappa_d^{-1} F_2^d/F_1^d$ with the anomalous magnetic moments normalized are relatively constant above $Q^2 \sim 1 \text{ GeV}^2$, they show a complicated behavior for lower Q^2 regions. Qattan and Arrington [36] elaborated the analysis of Ref. [35], taking into account explicitly the effects of two-photon exchange and uncertainties on the proton form factor and the neutron magnetic FFs. They found that the ratio of the up-quark EMFFs (G_E^u/G_M^u) has a roughly linear drop-off, while that of the down-quark EMFFs (G_E^d/G_M^d) showed a completely different dependence on Q^2 . As a result, for the flavor-decomposed FFs behave in a different way from the proton EMFFs. It was also pointed out in Ref. [36] that theoretical descriptions of the flavor-decomposed FFs seem nontrivial [38–41].

Being motivated by these recent experimental works, we want to investigate the flavor structure of the nucleon EMFFs within the framework of the self-consistent SU(3) chiral quark-soliton model (χ QSM) [42–44]. The χ QSM has described successfully various observables of the baryon octet and decuplet: mass splittings [45–47], form factors [48–55], magnetic moments [56–58], hyperon semileptonic decays [59–61], $\Delta \rightarrow N\gamma$ transitions [62–64], transversities of the nucleon [65–70], and parton distributions [71–78] including generalized parton distributions (GPDs) (see the following reviews [79–81] and references therein for more details). In particular, the Q^2 dependence of almost all form factors is well reproduced within the χ QSM, so that the strange-quark EMFFs [54] and the parity-violating (PV) asymmetries of polarized electron-proton scattering [53], which require nine different FFs (six EMFFs and three axial-vector FFs) with the same set of parameters, are in good agreement with experimental data [82–91]. Thus, it is worthwhile to examine the flavor structure of the nucleon EMFFs in detail. As mentioned, the nucleon EMFFs were already studied in the SU(3) χ QSM [48]. However, Praszalowicz *et al.* pointed out that the Gell-Mann-Nishijima relation was slightly broken in the old version of the χ QSM and proposed the symmetry-conserving quantization that makes the Gell-Mann-Nishijima relation well satisfied [92].

In this work, we present the results of the flavor-decomposed up- and down-quark EMFFs based on the SU(3) χ QSM with symmetry-conserving quantization employed. We first show the Dirac and Pauli FFs of the nucleon and then examine the Q^2 dependence of the up- and down-quark Dirac and Pauli FFs. The ratio of the flavor-decomposed Dirac and Pauli FFs will be discussed, compared with the recent experimental data [36]. We also reexamine the results of the strange EMFFs, since there are new experimental data from PV polarized electron-nucleon scattering. In particular, the G0 collaboration recently measured the parity-violating asymmetries in the backward angle [88], which was first predicted in Ref. [53].

In addition to the flavor decomposed EMFFs of the nucleon, we also investigate the charge and magnetization densities of the quark in a nucleon in the transverse plane. Together with the new experimental data for the nucleon EMFFs, the nucleon GPDs cast light on the concept of nucleon FFs [93–96]. In particular, they allow one to get access to the parton distributions in the transverse plane [97–99]. The nucleon EMFFs are directly related to the transverse charge and magnetization distributions of the quark inside a nucleon, as viewed from a light-front moving towards a transversely polarized nucleon [100, 101]. In fact, the transverse spin densities of the quarks inside a nucleon have been already studied in the χ QSM [70] and the results were in qualitative agreement with those of lattice QCD [102].

The present results of the transverse charge and magnetization densities are also found to be in good agreement with the empirical data extracted from the data.

The present work is sketched as follows. In Section II, we briefly explain the general formalism of the EMFFs of the nucleon and its flavor decomposition. In Section III, we show how to compute the EMFFs of the nucleon within the framework of the SU(3) χ QSM. In Section IV, we discuss the results of the flavor-decomposed FFs and their physical implications in comparison with the recent experimental data. We also present those of the transverse charge and magnetic distributions of the quark inside a nucleon. The final Section is devoted to summary and conclusion.

II. GENERAL FORMALISM

The matrix element of a flavor vector current between the two nucleon states is expressed in terms of the flavor Dirac and Pauli FFs

$$\langle N(p', s') | J_\mu^\chi(0) | N(p, s) \rangle = \bar{u}_N(p', s') \left[\gamma_\mu F_1^\chi(q^2) + i\sigma_{\mu\nu} \frac{q^\nu}{2M_N} F_2^\chi(q^2) \right] u_N(p, s), \quad (1)$$

where $J_\mu^\chi(0)$ represents the flavor vector current defined as

$$J_\mu^\chi(0) = \bar{\psi}(0) \lambda^\chi \gamma_\mu \psi(0). \quad (2)$$

χ denotes the flavor index, i.e. $\chi = 0, 3, 8$ for the flavor decomposition. Here, one has to bear in mind that λ^0 is considered to be a unity flavor matrix. Thus, the normalization $\{\lambda^a, \lambda^b\} = 2\delta^{ab}$ for λ^χ applies only to the Gell-Mann matrices with $\chi = 3$ and $\chi = 8$. γ_μ is the Dirac matrices and $u_N(p, s)$ the Dirac spinor for the nucleon with mass M_N , momentum p and the third component of its spin s . $\sigma_{\mu\nu}$ is the spin operator $i[\gamma_\mu, \gamma_\nu]/2$. q^2 stands for the square of the four momentum transfer $q^2 = -Q^2$ with $Q^2 > 0$. The flavor Dirac and Pauli FFs can be written in terms of the Sachs vector FFs, i.e., $G_E^\chi(Q^2)$ and $G_M^\chi(Q^2)$:

$$\begin{aligned} G_E^\chi(Q^2) &= F_1^\chi(Q^2) - \frac{Q^2}{4M_N^2} F_2^\chi(Q^2) \\ G_M^\chi(Q^2) &= F_1^\chi(Q^2) + F_2^\chi(Q^2). \end{aligned} \quad (3)$$

In the Breit frame, the Sachs-type form factors $G_E^\chi(Q^2)$ and $G_M^\chi(Q^2)$ are related to the time and space components of the flavor vector current, respectively:

$$\begin{aligned} G_E^\chi(Q^2) &= \langle N'(p') | \bar{\psi}(0) \gamma_0 \lambda^\chi \psi(0) | N(p) \rangle \\ G_M^\chi(Q^2) &= iM_N \epsilon_{ilk} \frac{q_l}{6q^2} \text{tr} \left(\langle p', \lambda' | \bar{\psi}(0) \gamma_i \lambda^\chi \psi(0) | p, \lambda \rangle \sigma_k \right). \end{aligned} \quad (4)$$

where σ_j stand for Pauli spin matrices. The $|\lambda\rangle$ is the corresponding spin state of the nucleon.

In SU(3) flavor the nucleon EMFFs are expressed in terms of the triplet and octet vector form factors

$$G_{E,M}^N(Q^2) = \frac{1}{2} \left(G_{E,M}^3 + \frac{1}{\sqrt{3}} G_{E,M}^8 \right), \quad (5)$$

while in flavor SU(2) they are expressed as

$$G_{E,M}^N(Q^2) = \frac{1}{2} \left(\frac{1}{3} G_{E,M}^0 + G_{E,M}^3 \right). \quad (6)$$

Although the same notation is used for the form factors, it will always follow from the context which flavor case is being addressed.

III. ELECTROMAGNETIC FORM FACTORS IN THE CHIRAL QUARK-SOLITON MODEL

The matrix element given in Eq. (4) can be evaluated in the SU(3) χ QSM. The model starts from the following low-energy effective partition function in Euclidean space

$$\mathcal{Z}_{\chi\text{QSM}} = \int \mathcal{D}\psi \mathcal{D}\psi^\dagger \mathcal{D}U \exp \left[- \int d^4x \bar{\Psi}^\dagger iD(U) \Psi \right] = \int \mathcal{D}U \exp(-S_{\text{eff}}[U]), \quad (7)$$

where ψ and U denote the quark and pseudo-Goldstone boson fields, respectively. Having integrated out the quark fields, we get the effective chiral action S_{eff} given as

$$S_{\text{eff}}(U) = -N_c \text{Tr} \ln iD(U), \quad (8)$$

where Tr represents the functional trace, N_c the number of colors, and $D(U)$ the Dirac differential operator

$$D(U) = \gamma_4(i\cancel{\partial} - \hat{m} - MU^{\gamma_5}) = -i\partial_4 + h(U) - \delta m \quad (9)$$

with

$$\delta m = \frac{-\bar{m} + m_s}{3} \gamma_4 \mathbf{1} + \frac{\bar{m} - m_s}{\sqrt{3}} \gamma_4 \lambda^8 = M_1 \gamma_4 \mathbf{1} + M_8 \gamma_4 \lambda^8. \quad (10)$$

In the present work we assume isospin symmetry, so that the current quark mass matrix is defined as $\hat{m} = \text{diag}(\bar{m}, \bar{m}, m_s) = \bar{m} + \delta m$. The mass δm containing the strange current quark mass m_s will be treated as a perturbation. The SU(3) single-quark Hamiltonian $h(U)$ is expressed as

$$h(U) = i\gamma_4 \gamma_i \partial_i - \gamma_4 M U^{\gamma_5} - \gamma_4 \bar{m}, \quad (11)$$

where U^{γ_5} stands for the chiral field for which we assume Witten's embedding of the SU(2) soliton into SU(3)

$$U^{\gamma_5}(x) = \begin{pmatrix} U_{\text{SU}(2)}^{\gamma_5}(x) & 0 \\ 0 & 1 \end{pmatrix} \quad (12)$$

with the SU(2) pion field $\pi^i(x)$ as

$$U_{\text{SU}(2)}^{\gamma_5} = \exp(i\gamma^5 \tau^i \pi^i(x)) = \frac{1 + \gamma^5}{2} U_{\text{SU}(2)} + \frac{1 - \gamma^5}{2} U_{\text{SU}(2)}^\dagger. \quad (13)$$

The integration over the pion field U in Eq. (7) can be performed by the saddle-point approximation in the large N_c limit due to the N_c factor in Eq. (8). The SU(2) pion field U is written as the most symmetric hedgehog form

$$U_{\text{SU}(2)} = \exp[i\gamma_5 \hat{\mathbf{n}} \cdot \boldsymbol{\tau} P(r)], \quad (14)$$

where $P(r)$ is the radial profile function of the soliton.

The nucleon state $|N(p, s)\rangle$ in Eq. (1) is defined as an Ioffe-type current consisting of N_c valence quarks in the χ QSM:

$$|N(p, s)\rangle = \lim_{x_4 \rightarrow -\infty} \frac{1}{\sqrt{\mathcal{Z}}} e^{ip_4 x_4} \int d^3 \mathbf{x} e^{i\mathbf{p} \cdot \mathbf{x}} J_N^\dagger(x) |0\rangle \quad (15)$$

with

$$J_N(x) = \frac{1}{N_c!} \Gamma_N^{b_1 \dots b_{N_c}} \varepsilon^{\beta_1 \dots \beta_{N_c}} \psi_{\beta_1 b_1}(x) \dots \psi_{\beta_{N_c} b_{N_c}}(x), \quad (16)$$

where the matrix $\Gamma_N^{b_1 \dots b_{N_c}}$ carries the hypercharge Y , isospin I, I_3 and spin s, s_3 quantum numbers of the baryon and the b_i and β_i denote the spin-flavor and color indices, respectively. Having minimized the action in Eq. (8), we derive an equation of motion which is solved self-consistently with respect to the function $P(r)$ in Eq. (14). The corresponding unique solution U_c is called the classical chiral soliton.

The next step is to quantize the classical soliton. This can be done by quantizing the rotational and translational zero-modes of the soliton. The rotations and translations of the soliton are implemented by

$$U(\mathbf{x}, t) = A(t) U_c(\mathbf{x} - \mathbf{z}(t)) A^\dagger(t), \quad (17)$$

where $A(t)$ denotes a time-dependent SU(3) matrix and $\mathbf{z}(t)$ stands for the time-dependent translation of the center of mass of the soliton in coordinate space. The rotational velocity of the soliton $\Omega(t)$ is defined as

$$\Omega = \frac{1}{i} A^\dagger \dot{A} = \frac{1}{2i} \text{Tr}(A^\dagger \dot{A} \lambda^\alpha) \lambda^\alpha = \frac{1}{2} \Omega_\alpha \lambda^\alpha. \quad (18)$$

Treating $\Omega(t)$ and δm perturbatively with a slowly rotating soliton assumed and with δm regarded as a small parameter, we obtain the collective Hamiltonian of the χ QSM [47] expressed as

$$H_{coll} = H_{\text{sym}} + H_{\text{sb}} , \quad (19)$$

$$H_{\text{sym}} = M_c + \frac{1}{2I_1} \sum_{i=1}^3 J_i J_i + \frac{1}{2I_2} \sum_{a=4}^7 J_a J_a, \quad (20)$$

$$H_{\text{sb}} = \frac{1}{\bar{m}} M_1 \Sigma_{SU(2)} + \alpha D_{88}^{(8)}(A) + \beta Y + \frac{\gamma}{\sqrt{3}} D_{8i}^{(8)}(A) J_i . \quad (21)$$

Diagonalizing the collective Hamiltonian, we find the octet baryon states

$$|N_8\rangle = |8_{1/2}, N\rangle + c_{\overline{10}} \sqrt{5} |\overline{10}_{1/2}, N\rangle + c_{27} \sqrt{6} |27_{1/2}, N\rangle, \quad (22)$$

where $c_{\overline{10}}$ and c_{27} are mixing parameters expressed as

$$c_{\overline{10}} = -\frac{I_2}{15} \left(\alpha + \frac{1}{2} \gamma \right), \quad c_{27} = -\frac{I_2}{25} \left(\alpha - \frac{1}{6} \gamma \right), \quad (23)$$

and α and γ represent the effects of $SU(3)$ symmetry breaking written as

$$\alpha = \frac{1}{\bar{m}} \frac{1}{\sqrt{3}} M_8 \Sigma_{SU(2)} - \frac{N_c}{\sqrt{3}} M_8 \frac{K_2}{I_2}, \quad \gamma = -2\sqrt{3} M_8 \left(\frac{K_1}{I_1} - \frac{K_2}{I_2} \right). \quad (24)$$

The moments of inertia I_1, I_2 and K_1, K_2 can be found, for example, in Ref. [47, 80]. Note that the nucleon state is no more a pure octet state but is a state mixed with higher representations as shown in Eq. (22). A detailed formalism for the zero-mode quantization can be found in Refs. [47, 48, 80].

IV. RESULTS AND DISCUSSION

In this Section, we present and discuss the results. In Refs. [48, 80], one can find a detailed description as to how the form factors can be obtained numerically. We briefly summarize it here before we discuss the numerical results. The parameters existing in the model are the constituent quark mass, the current quark mass \bar{m} , strange quark mass m_s , and the cutoff mass Λ of the proper-time regularization. However, not all of them are free parameters but can be fixed in the mesonic sector without any ambiguity. In fact, this is a merit of the χ QSM in which mesons and baryons can be treated on an equal footing. For a given M the regularization cut-off parameter Λ and the current quark mass \bar{m} in the Lagrangian are fixed to the pion decay constant $f_\pi = 93$ MeV and the physical pion mass $m_\pi = 140$ MeV, respectively. The strange current quark mass is taken to be $m_s = 180$ MeV which approximately reproduces the kaon mass. Though the constituent quark mass M can be regarded as a free parameter, it is also more or less fixed. The experimental proton electric charge radius is best reproduced in the χ QSM with the constituent quark mass $M = 420$ MeV. Moreover, the value of 420 MeV is known to yield the best fit to many baryonic observables [80]. Thus, all the numerical results in the present work are obtained with this value of M .

All the results presented in the following were computed completely within the model, in the same level of approximation, to keep consistency. In particular, magnetization observables are presented not in terms of nucleon magneton but, instead, in terms of the model nuclear magneton, i.e. defined as the model value for the nucleon mass, which, at this level of approximation used in this work, is

$$M_N = 1250 \text{ MeV}. \quad (25)$$

This value is not corrected from a spurious center of mass motion stemming from the mean field approach. Although it is possible to correct such contributions and obtain a nucleon mass close to its experimental value, such corrections are not applied to the form factors in the following.

A. Sachs EM form factors

The Sachs EM form factors [115, 116] are the most common form to encompass information about the electromagnetic structure of the nucleon. On the one hand, these form factors make it possible to express the cross section for elastic electron-proton scattering in the one-photon exchange approximation, without mixed terms ($G_E G_M$) in a form

suitable for the separation of the electric and magnetic form factors. That is not the case when the cross section is expressed in terms of the Dirac and Pauli form factors (1), where the mixed terms ($F_1 F_2$) occur. Even with the more recent polarization transfer methods [118], the measured ratio between the longitudinal and transverse polarization components is expressed in terms of the Sachs form factors ratio $\mu G_E/G_M$.

On the other hand, the Sachs form factors have the appeal that in the Breit frame they may be apparently interpreted as the Fourier transform of the charge and magnetization distributions inside the nucleon. Such expectation comes from the fact that in the Breit frame the proton does not exchange energy with the virtual photon with momentum $(0, \mathbf{q})$. At a specific space-like $Q^2 = -\mathbf{q}^2 < 0$ invariant momentum transfer, the time and space components of the electromagnetic current, associated with the electric and magnetic form factors respectively, resemble the classical non-relativistic current density. Hence the Sachs EM form factors are directly related to the charge and magnetization distributions by the Fourier transform. However, these relations are supposedly non-relativistic in nature due to the Q^2 dependence of the Breit-frame. Both the preceding features of the Sachs form factors are currently under scrutiny, as mentioned in Introduction. Discrepancies in the experimental results from the elastic ep cross section and polarization transfer studies called for the inclusion of new aspects of elastic electron proton scattering, such as the two-photon exchange [19]. The connection between form factors and densities, even apart from the non-relativistic limitation, has also been revised on general grounds [100, 105].

The electromagnetic form factors computed in the χ QSM are obtained as Fourier transforms of the charge and magnetization densities derived from the model. These densities are obtained in the rest frame of the nucleon and, therefore, the validity of the results for the form factors is restricted to small momentum transfers $Q^2 \ll M_N^2$. Improving this situation by taking into account relativistic boost effects explicitly in the model has proven to be rather difficult. However, we will adopt the simple prescription of treating the form factors as Lorentz scalars so that we can gain insight into the impact of such effects on the EM form factors from the model.

In the Breit frame the initial nucleon state has three-momentum $-\mathbf{q}_B/2$ and the final state has three-momentum $\mathbf{q}_B/2$. Since there is no transfer of energy, the invariant four-momentum transfer can be written as $q_B^2 = -\mathbf{q}_B^2 = -Q^2 < 0$. In the reference frame in which the nucleon is initially at rest, where the exchanged photon four-momentum is (ω, \mathbf{q}) , the space-like invariant momentum transfer $Q^2 = \mathbf{q}^2 - \omega^2$ is given as

$$Q^2 = \frac{\mathbf{q}^2}{1 + \frac{Q^2}{4M^2}} = \mathbf{q}_B^2, \quad (26)$$

which contains the Lorentz-boost factor γ relating the rest to the Breit-frame

$$\gamma = \frac{1}{\sqrt{1 + \frac{Q^2}{4M^2}}} = \frac{1}{\sqrt{1 + \tau}} \quad (27)$$

with

$$\tau = Q^2/(4M^2). \quad (28)$$

It is then possible to write for the form factors

$$G^{\text{rel}}(Q^2) \equiv G^{\text{Breit}}(Q^2) = G^{\text{rest}}(Q^2/\gamma^2), \quad (29)$$

with the Lorentz contraction effects considered. In the following, the results for the Sachs EM form factors of the nucleon obtained directly from the χ QSM will have no special designation and those yielded from Eq. 29 will be distinguished by the superscript ‘rel’.

It is worth emphasizing that M entering Eq. (27) is not a parameter, but it is given by Eq. (25), i.e. it is the mass of the nucleon obtained from the model. Most of the results presented here would improve if a somewhat higher value of M were to be considered. However, such a high value would be hard to be justified within the model. Such improvement is easily understood by noticing both that, as most of the Figures show, the phenomenological data lie between the model results in the rest frame and the corresponding ones boosted to the Breit frame and also that the Breit frame results approach the rest frame ones as the boost mass increases.

The limitation of using the rest, center-of-mass reference frame in model calculations of form factors is common in many models of hadron structure. Similar approaches to Eq. (29) have been suggested before, mostly in the more general form

$$G_E^{\text{Breit}}(Q^2) = (\gamma^{-2})^{\lambda_E} G_E^{\text{rest}}(Q^2/\gamma^2), \quad (30)$$

$$G_M^{\text{Breit}}(Q^2) = (\gamma^{-2})^{\lambda_M} G_M^{\text{rest}}(Q^2/\gamma^2). \quad (31)$$

This boost prescription translates mathematically into a mapping of the domain of Q^2 from $[0, 4M^2[$ to $[0, \infty[$, thus the domain of validity of the model results being extended. However, since the model results usually predict $G_M^{\text{rest}}(4M^2) \neq 0$ and the χ QSM has a normalization scale below 1 GeV, which is given by the cutoff parameter Λ , the Q^{-4} scaling behavior predicted by perturbative QCD is not necessarily satisfied. Hence, λ_E and λ_M , which do not need to be equal, may be used according to the model and the scaling behavior of the form factors. It is also possible to treat the boost mass in (27) as a parameter with the meaning of an effective mass. These approaches were taken first in a cluster quark model [119], $\lambda_E = \lambda_M = 1$ being used. On the other hand, a later study [104] considered an improved scaling of the form factors at very large Q^2 in favor of $\lambda_E = \lambda_M = 2$. In the context of the Skyrme model [120, 121] the preferred choice was $\lambda_E = 0$ and $\lambda_M = 1$, based on the different Lorentz transformation of the scalar and vector densities. In a more recent work [103], $\lambda_E = \lambda_M = 2$ was chosen in extracting the charge and magnetization densities from the Sachs EM form factors. In this work, we select $\lambda_E = \lambda_M = 0$, which improves much the form factors with regards to the experimental values. At the same time, since the model aims at the low Q^2 behavior of form factors, there is no reason to force the high Q^2 behavior by choosing higher values for λ .

The Q^2 interval used in the results is $[0, 5]$ GeV². This interval is larger than the expected domain of validity of the model results, which are expected to hold up to $Q^2 \ll M^2$ for the results in the rest frame results and up to $Q^2 \simeq M^2$ for those boosted to the Breit frame. The interval chosen allows one to observe the trend for higher Q^2 values, as well as that of the phenomenological data against the expected scaling behavior. We note that the model results do not necessarily have any predictability regarding the onset of the scaling.

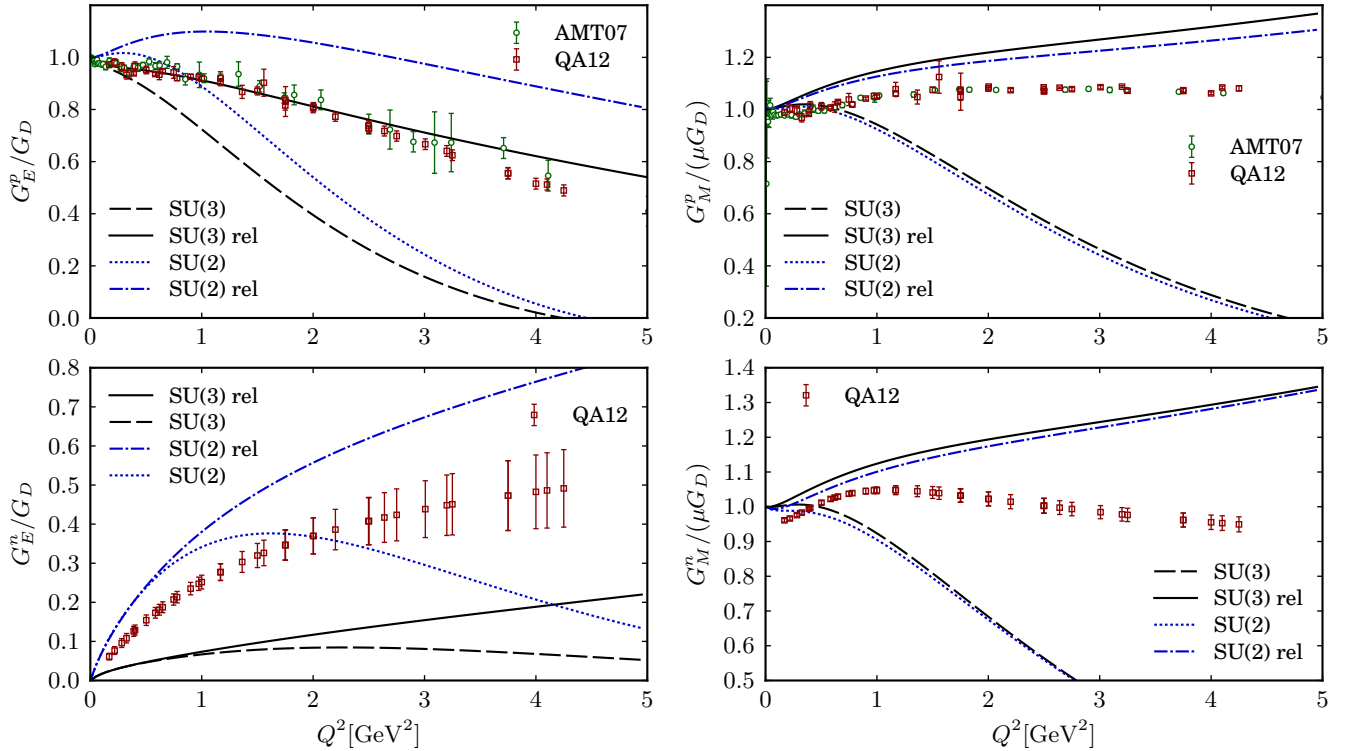


Figure 1. Ratios of the nucleon EMFFs to the corresponding dipole parameterizations. As explained in the text, SU(3) stands for the model results in flavor SU(3) and the SU(2) for the flavor SU(2) results. The corresponding recoil corrected form factors are denoted by ‘rel’. The phenomenological data are taken from Refs. [18] (AMT07) and [36, 37] (QA12).

In Fig. 1, we draw the ratios of the EMFFs from the model to the corresponding dipole parameterization defined as

$$G_D(Q^2) = \frac{1}{\left(1 + \frac{Q^2}{\Lambda_D^2}\right)^2} \quad (32)$$

with $\Lambda_D^2 = 0.71$ GeV². The phenomenological data shown in Fig 1 are taken from the two analyses [18, 36] in which the Sachs EMFFs were consistently extracted from the cross section of elastic electron-proton scattering and

the polarization transfer experimental data. While the proton electric FF with relativistic corrections explain the data very well, the proton magnetic one turns out to be slightly overestimated. On the other hand, the neutron electric FF deviates from the data. However, we want to mention that the neutron electric FF is rather sensitive to the soliton tail, because it is defined as the subtraction of the triplet and octet vector currents. As shown in Fig 1, the SU(3) results are rather different from those in SU(2), the reason stemming, at least partially, from the strange quark contribution to the neutron electric FF. Because of the embedding of the SU(2) soliton into SU(3) as shown in Eq.(12), the contribution of the strange quark has the same asymptotic behavior of the nonstrange quarks. The effects due to different asymptotic tails were discussed in Ref. [50] in detail in the context of the strange vector FFs of the nucleon. Thus, in a sense, a true answer may be found between the SU(2) and the SU(3) results. The neutron magnetic FF seems to deviate from the data as Q^2 increases.

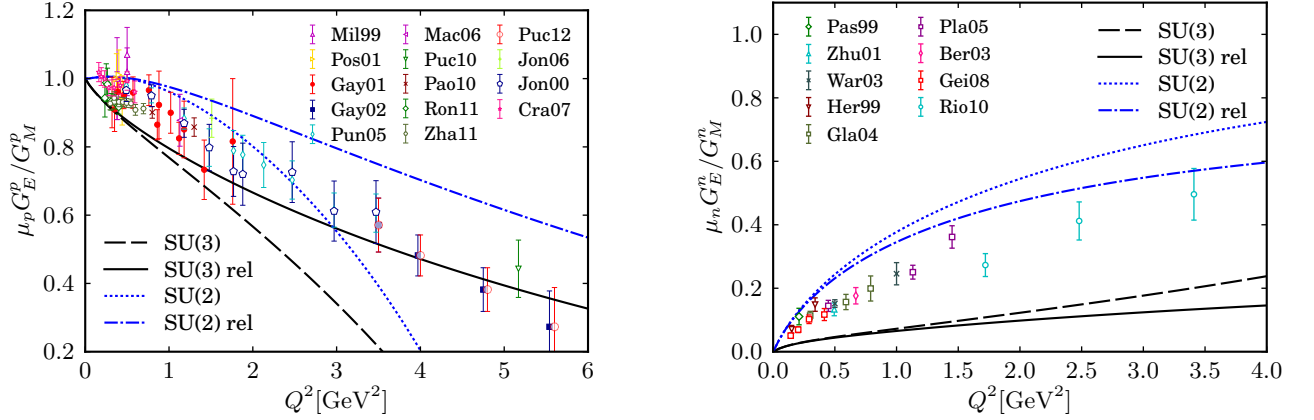


Figure 2. The ratio of the proton magnetic FF to the electric FF: $\mu_p G_E^p / G_M^p$ in the left panel. The experimental data are taken from Mil99 [107], Pos01 [108], Gay01 [2], Gay02 [3], Pun05 [4], Mac06 [109], Puc10 [5], Pao10 [110], Ron11 [7], Zha11 [8], Puc12 [111], Jon06 [112], Jon00 [1], Cra07 [113]. Neutron $\mu_n G_E^n / G_M^n$ ratio in the right panel compared to the data from recent experiments: Pas99 [25], Zhu01 [27], War03 [29], Gei08 [32], Her99 [114], Gla04 [30], Pla05 [31], Ber03 [28], Rio10 [34]. Notations are the same as Fig. 1.

The experimental data show that the ratio $\mu_p G_E^p / G_M^p$ already starts to fall near $Q^2 \approx 0$, which indicates that the charge and magnetization distributions are different from each other, even though their charge radii are of almost the same order. Indeed, they have distinctive features, as will be discussed later in detail. In the left panel of Fig. 2, the results of the ratio of the proton magnetic FF to the electric FF are depicted in comparison with the experimental data from the recoil polarization experiments $p(\vec{e}, e' \vec{p})$ [1–5, 7, 8, 107–111] and the experiments with a polarized target $\vec{p}(\vec{e}, e' \vec{p})$ [112, 113]. The experimental data indicate that G_E^p falls off faster than G_M^p . As shown in Fig. 2, the SU(3) results can describe the general tendency of the data, whereas those of SU(2) seem overestimated, as Q^2 increases. The right panel of Fig. 2 plots the results for the ratio $\mu_n G_E^n / G_M^n$, compared with the experimental data taken from $\vec{d}(\vec{e}, en)p$ [25, 27, 29, 32] and from $d(\vec{e}, e' \vec{n})p$ [30, 31, 114] and $^3\text{He}(\vec{e}, e' n)$ scatterings [28, 34]. The general tendency of the present results are in line with the experimental data: $\mu_n G_E^n / G_M^n$ increases systematically as Q^2 increases. However, the SU(2) results are slightly overestimated in comparison with the data, while the SU(3) results turn out to be smaller than the data. However, as discussed above, the electric FF of the neutron is quite sensitive to the asymptotics of the soliton tail, and thus, the difference between the SU(2) and SU(3) results may be regarded as a model uncertainty.

B. Flavor Sachs form factors

In order to decompose the proton EMFFs into the flavor ones, we need to compute the singlet vector form factors of the proton. Then, we are able to express the flavor-decomposed EMFFs of the proton in terms of the singlet, triplet, and octet FFs of the proton:

$$G_{E,M}^u(Q^2) = \frac{1}{2} \left(\frac{2}{3} G_{E,M}^{(0)}(Q^2) + G_{E,M}^{(3)}(Q^2) + \frac{1}{\sqrt{3}} G_{E,M}^{(8)}(Q^2) \right),$$

$$\begin{aligned}
G_{E,M}^d(Q^2) &= \frac{1}{2} \left(\frac{2}{3} G_{E,M}^{(0)}(Q^2) - G_{E,M}^{(3)}(Q^2) + \frac{1}{\sqrt{3}} G_{E,M}^{(8)}(Q^2) \right), \\
G_{E,M}^s(Q^2) &= \frac{1}{3} \left(G_{E,M}^{(0)}(Q^2) - \sqrt{3} G_{E,M}^{(8)}(Q^2) \right),
\end{aligned} \tag{33}$$

where we have suppressed the corresponding quark charge. The normalizations at $Q^2 = 0$ are performed with $\mu_q = G_M^q(0)$ as

$$\begin{aligned}
G_E^u(0) &= 2, & G_E^d(0) &= 1, & G_E^s(0) &= 0, \\
\mu_u &= 3.22 \mu_N, & \mu_d &= -0.73 \mu_N, & \mu_s &= 0.10 \mu_N,
\end{aligned} \tag{34}$$

for the proton in SU(3) and as

$$\begin{aligned}
G_E^u(0) &= 2, & G_E^d(0) &= 1 \\
\mu_u &= 3.46 \mu_N, & \mu_d &= -0.95 \mu_N,
\end{aligned} \tag{35}$$

in flavor SU(2).

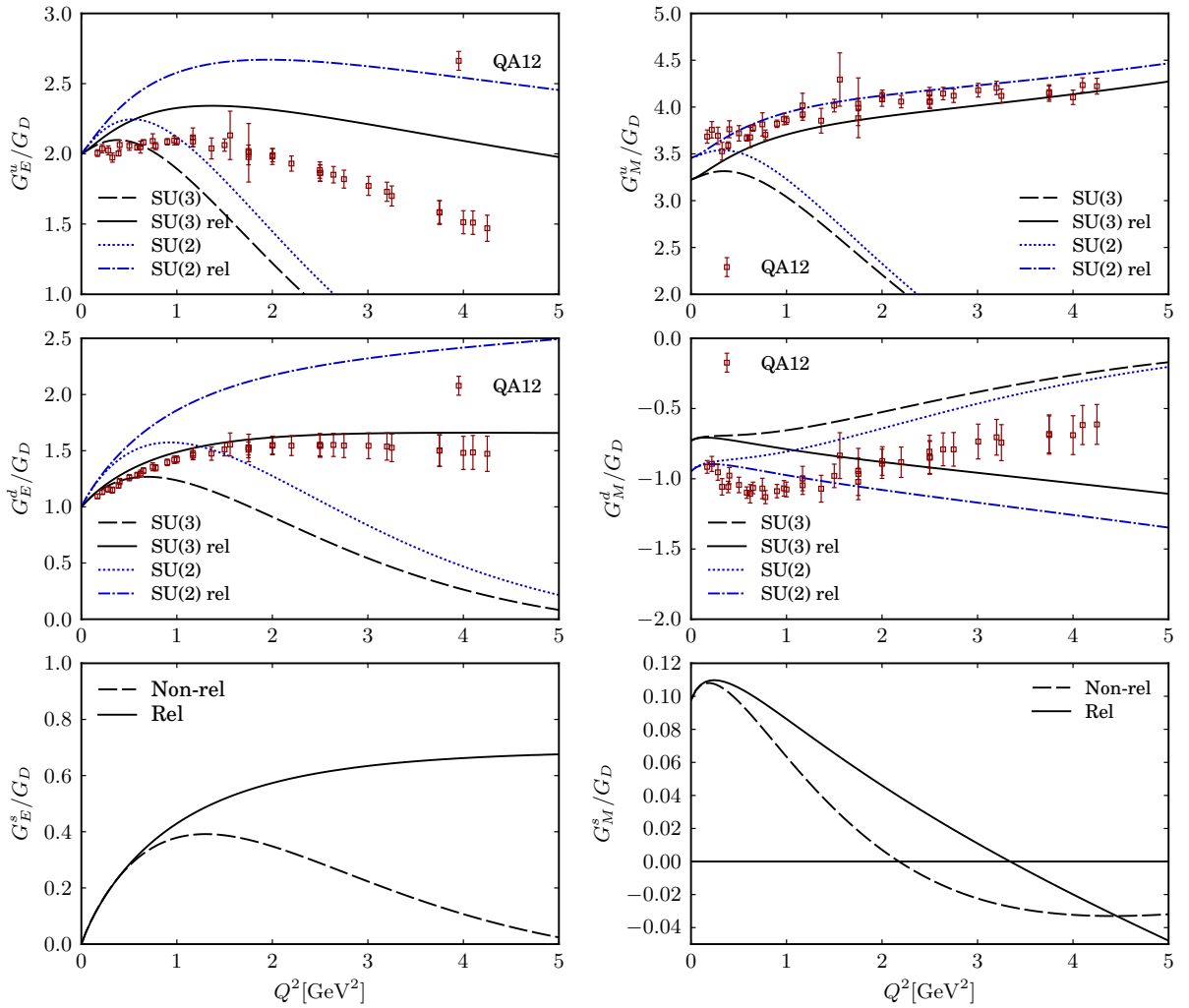


Figure 3. Ratios of the nucleon Sachs flavor FFs to the dipole parameterizations (Eq. (32)). The u quark FFs in the upper panel, the d quark FFs in the middle panel, and the strange ones in the lower panel. The phenomenological data are taken from Refs. [36, 37] (QA12). Notations are the same as in Fig. 1.

The Sachs FFs for the different quark flavors are presented in Fig. 3, as obtained from Eqs. (33), in comparison with the phenomenological data taken from Refs. [36, 37] whose normalizations at $Q^2 = 0$ are given as $G_M^u = 3.67 \mu_N$ and

$G_M^d = -1.03 \mu_N$. The up magnetic FF and down electric FF are more or less well reproduced, with the relativistic effects taken into account. When they are switched off, the results deviates from the data as Q^2 increases, which is understandable. The up electric FF from the SU(3) model with the relativistic effects show qualitatively a similar feature to the data, whereas the down magnetic FFs seem to differ from them. In this case, however, it was observed that the boost mass around 1.8 GeV^2 reproduces them very well. It also improves the other FFs but as already stated the boost mass would have to be understood as an effective mass, i.e. a parameter beyond the model. Since there are no experimental data yet for the strange EMFFs, the down panels of Fig. 3 show the predictions of the present model for the strange EMFFs.

C. Dirac and Pauli form factors

The Dirac (F_1) and Pauli (F_2) FFs are expressed in terms of the Sachs EM FFs defined in Eq. (3), i.e.

$$\begin{aligned} F_1(Q^2) &= \frac{G_E + \tau G_M}{1 + \tau} \\ F_2(Q^2) &= \frac{G_M - G_E}{1 + \tau}, \end{aligned} \quad (36)$$

where τ is given in Eq. (28). At $Q^2 = 0$ these FFs have the following results:

$$\begin{aligned} F_1^p(0) &= 1, & F_1^n(0) &= 0, \\ \kappa_p &= 1.36, & \kappa_n &= -1.59 \end{aligned} \quad (37)$$

in flavor SU(3), and

$$\begin{aligned} F_1^p(0) &= 2, & F_1^n(0) &= 1, \\ \kappa_p &= 1.62, & \kappa_n &= -1.78. \end{aligned} \quad (38)$$

in flavor SU(2). The experimental values for the anomalous magnetic moments are given as

$$\kappa_p = 1.793, \quad \kappa_n = -1.913. \quad (39)$$

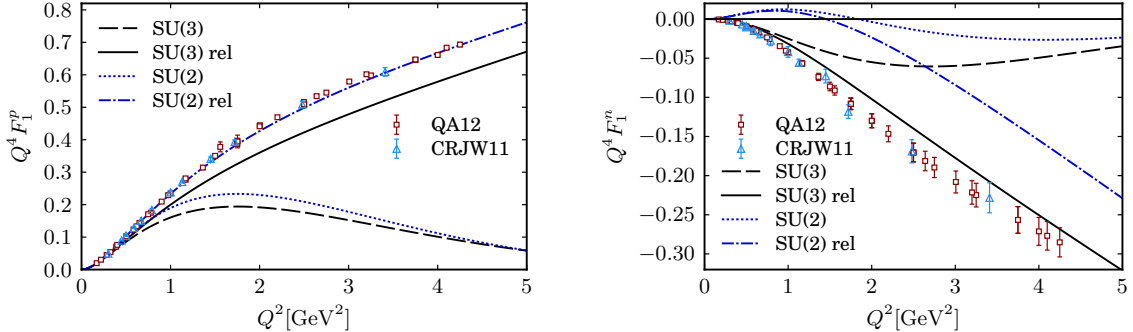


Figure 4. Dirac FFs F_1 of the proton and the neutron, scaled with Q^4 . The experimental data are taken from Refs. [35] (CRJW11) and [36, 37]. Notations are the same as in Fig. 1.

As mentioned in Introduction, pQCD with factorization schemes [21] predicts that the nucleon Dirac FFs are scaled as $1/Q^4$. It indicates that $Q^4 F_1(Q^2)$ becomes asymptotically constant. Figure 4 shows the results for the nucleon Dirac FFs with Q^4 factor in comparison with the experimental data [35–37]. Interestingly, the Q^2 dependence of $Q^4 F_1^p(Q^2)$ are well explained within the SU(2) model with the relativistic effects, while those from the corresponding SU(3) model seem slightly underestimated. As for $Q^4 F_1^n(Q^2)$, the results of the SU(3) model with the relativistic effects can only describe the data. With these relativistic corrections turned off, we observe that $Q^4 F_1(Q^2)$ are quantitatively described up to $(0.8 - 1) \text{ GeV}^2$, which seems reasonable.

The Pauli FFs show the scaling of $1/Q^6$, based on pQCD with factorization schemes [21], being different from the Dirac FFs. In Fig. 5, $Q^6 F_2(Q^2)$ are depicted for both the proton and the neutron. In this case, both the SU(2) and SU(3) models without the relativistic effects describe the data very well up to $Q^2 \simeq 1 \text{ GeV}^2$. As Q^2 further increases,

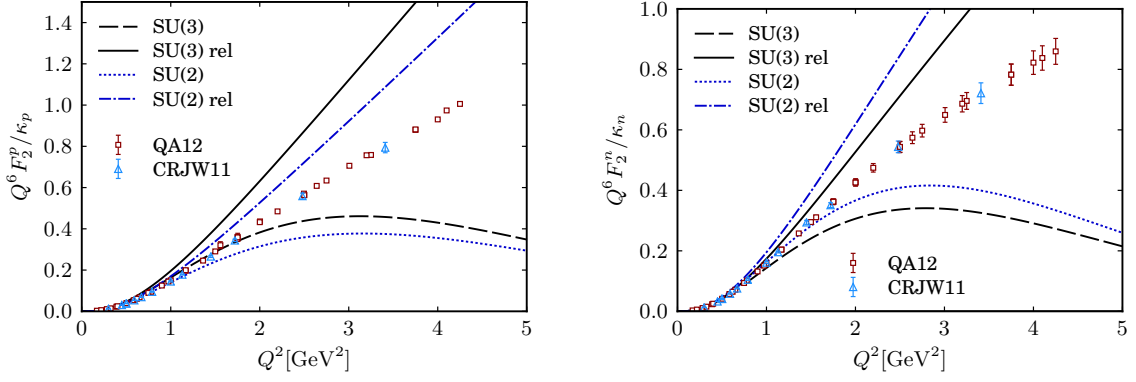


Figure 5. Pauli FFs F_1 of the proton and the neutron, scaled with Q^4 . The experimental data are taken from Refs. [35] (CRJW11) and [36, 37]. Notations are the same as in Fig. 1.

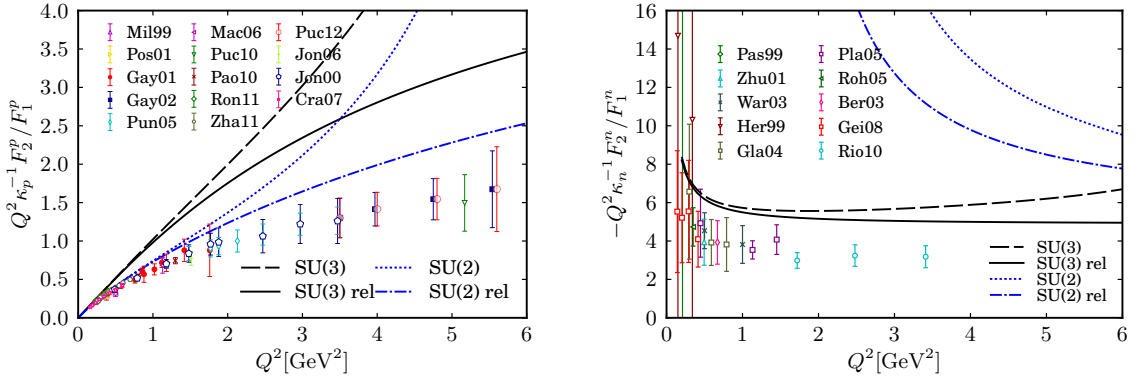


Figure 6. Ratios $Q^2 \kappa^{-1} F_2 / F_1$ for the proton and the neutron in the left and right panels, respectively. The experimental data are taken from those used in Fig. 2. Notations are the same as in Fig. 1.

the present results start to deviate from the data. However, those of $Q^6 F_2(Q^2)$ for both the proton and the neutron seem overestimated with the relativistic effects, compared with the experimental data.

In Fig. 6 we show the model results for the ratios $Q^2 \kappa^N F_2^N / F_1^N$ for the proton (left panel) and the neutron (right panel). The experimental data in Fig. 6 are taken from those used in Fig. 4 and in Fig. 5. Note that the ratio of the Pauli FF to the Dirac one is related to the ratio of the EMFFs as follows:

$$\frac{F_2}{F_1} = \frac{1 - R/\mu}{\tau + R/\mu}. \quad (40)$$

While the qualitative tendencies of $Q^2 \kappa^N F_2^N / F_1^N$ are described, the results turn out to be larger than the experimental data, in particular, in the case of the proton.

D. Flavor dcomposition of the Dirac and Pauli form factors

The flavor-decomposed Dirac (F_1^q) and Pauli (F_2^q) FFs are expressed as

$$\begin{aligned} F_{1,2}^u &= 2F_{1,2}^p + F_{1,2}^n + F_{1,2}^s, \\ F_{1,2}^d &= F_{1,2}^p + 2F_{1,2}^n + F_{1,2}^s, \end{aligned} \quad (41)$$

in flavor SU(3). In flavor SU(2), the up and down Dirac and Pauli FFs are simply written in terms of the corresponding proton and neutron FFs.

$$F_{1,2}^u = 2F_{1,2}^p + F_{1,2}^n,$$

$$F_{1,2}^d = F_{1,2}^p + 2F_{1,2}^n. \quad (42)$$

Note that, however, the SU(3) results are not reduced to the SU(2) ones just by merely turning off the effects of the strange quark. The normalizations of the Dirac and Pauli FFs at $Q^2 = 0$ are given as follows:

$$\begin{aligned} F_1^u(0) &= 2, & F_1^d(0) &= 1, & F_1^s(0) &= 0, \\ \kappa_u &= 1.22, & \kappa_d &= -1.73, & \kappa_s &= 0.10. \end{aligned} \quad (43)$$

in flavor SU(3) and

$$\begin{aligned} F_1^u(0) &= 2, & F_1^d(0) &= 1, \\ \kappa_u &= 1.46, & \kappa_d &= -1.95 \end{aligned} \quad (44)$$

The phenomenological values for the anomalous magnetic moments are yielded as

$$\kappa_u = 1.673, \quad \kappa_d = -2.033. \quad (45)$$

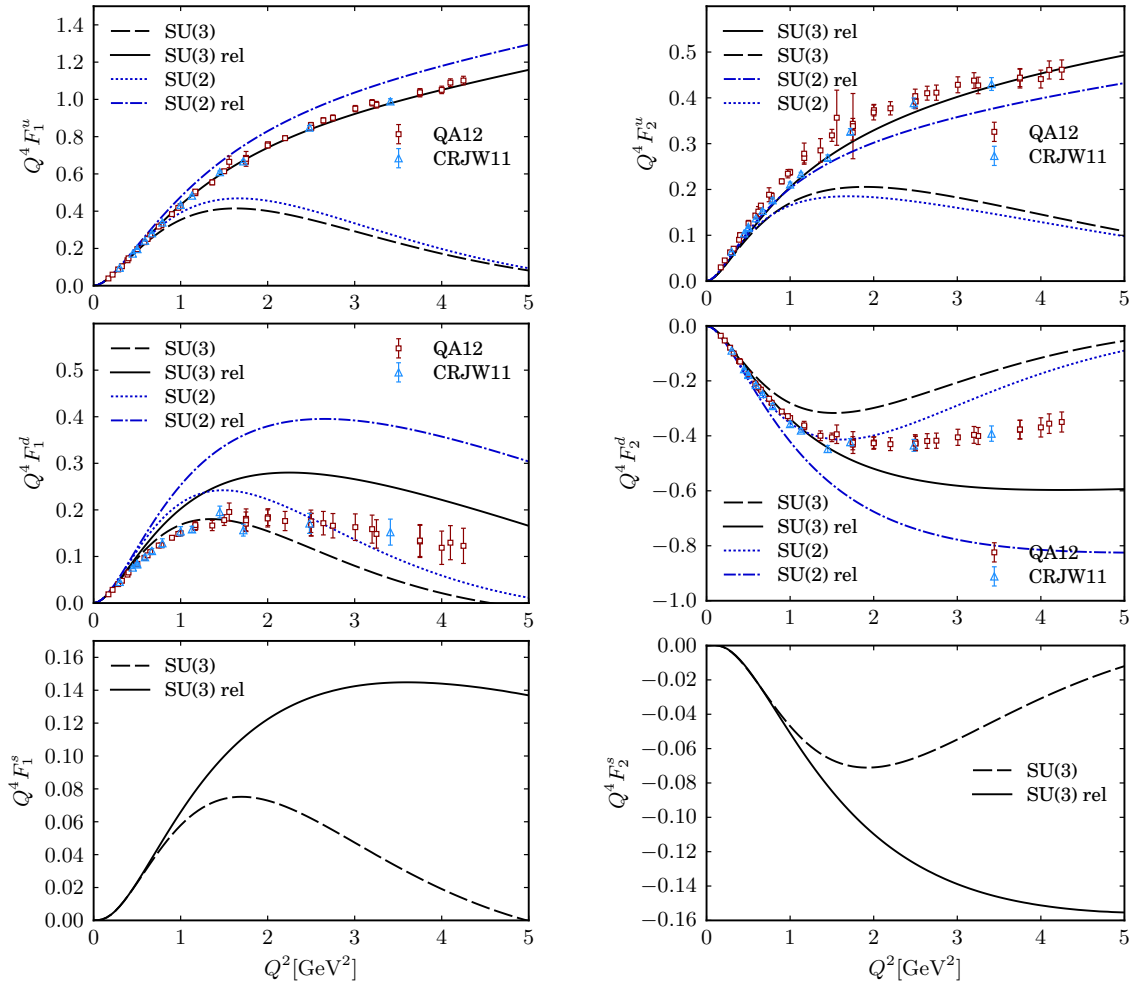


Figure 7. The flavor-decomposed Dirac and Pauli FFs scaled with Q^4 : The up FFs in the upper panel, the down ones in the middle panel, and the strange FFs in the lower panel. The experimental data are taken from Refs. [35–37]. Notations are the same as in Fig. 1.

In Fig. 7, we draw the results of $Q^4 F_{1,2}^q$ for the up (u), down (d) and strange (s) quarks, respectively. The experimental data clearly exhibit different Q^2 dependencies of $F_{1,2}^u$ and $F_{1,2}^d$. The present results for both the up and down quarks describe the data very well below $Q^2 \simeq 1 \text{ GeV}^2$ as in the case of the proton and neutron FFs (see

Figs. 4 and 5). When the relativistic effects are included, the results for the up Dirac and Pauli FFs are in remarkable agreement with the data. However, as for the down FFs, the results with the relativistic effects are overestimated in magnitude. We clearly see the relativistic effects in the strange FFs.

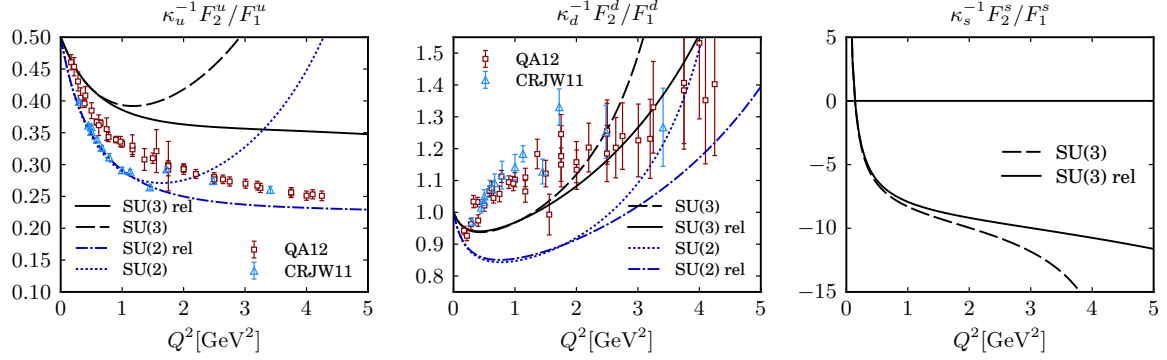


Figure 8. The ratios $\kappa_q^{-1} F_2^q / F_1^q$ for the up, down, and strange flavors. The experimental data are taken from Refs. [35–37]. Notations are the same as in Fig. 1.

The ratios of the Pauli FFs to the Dirac FFs $\kappa_q^{-1} F_2^q / F_1^q$ are depicted in Fig. 8 for each flavor. The SU(2) result for $\kappa_u^{-1} F_2^u / F_1^u$ with the relativistic effects describes very well the data from Ref. [35], while it is underestimated, compared with those of Ref. [36]. However, both the SU(2) and SU(3) results with the relativistic effects show that F_2^u / F_1^u falls rapidly at lower Q^2 but decreases more slowly, as Q^2 increases like in the experimental data. The SU(2) model results without the relativistic effects explain the data below 1 GeV^2 . The down panel of Fig. 8 shows the prediction for the strange quark.

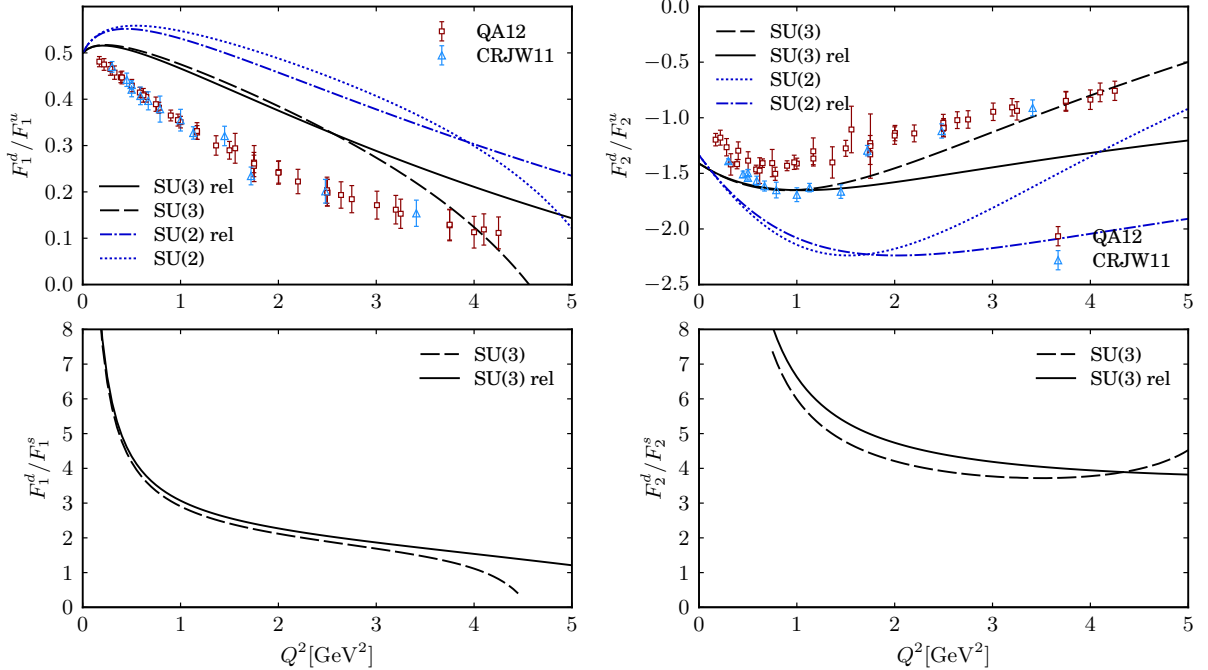


Figure 9. Ratios of the down (d) FFs to the up (u) and strange (s) FFs. The experimental data are taken from Refs. [35–37]. Notations are the same as in Fig. 1.

As shown in Fig. 7, the Dirac and Pauli FFs for the up and down quarks exhibit different Q^2 dependencies. Thus, it is also of significant interest to examine the ratios F_1^d / F_1^u and F_2^d / F_2^u . The corresponding results are depicted in the upper panel of Fig. 9. Interestingly, they are qualitatively similar to the experimental data, which implies that

the present model yields consistently the faster falloff of the down quark FFs than that of the up quark FFs. On the other hand, as Q^2 increases, F_1^d/F_1^s and F_2^d/F_2^s fall off quite slowly, which indicates that the Q^2 dependence of the strange quark FFs becomes more or less similar to that of the down quark FFs.

E. Transverse charge densities

We are now in a position to discuss the quark transverse charge densities inside both unpolarized and polarized nucleons. The traditional charge and magnetization densities in the Breit framework are defined ambiguously because of the Lorentz contraction of the nucleon in its moving direction [98, 103]. To avoid this ambiguity one can define the quark charge densities in the transverse plane. Then, they provide essential information on how the charges and magnetizations of the quarks are distributed in the transverse plane inside the nucleon. When the nucleon is unpolarized, the quark transverse charge density is defined as the two-dimensional Fourier transform of the nucleon Dirac FFs

$$\begin{aligned}\rho_{\text{ch}} &= \frac{1}{(2\pi)^2} \int d^2q e^{i\mathbf{q}\cdot\mathbf{b}} F_1(Q^2) \\ &= \int_0^\infty \frac{dQ}{2\pi} Q J_0(Qb) F_1(Q^2) = \int_0^\infty \frac{dQ}{2\pi} Q J_0(Qb) \frac{G_E(Q^2) + \tau G_M(Q^2)}{1 + \tau},\end{aligned}\quad (46)$$

where b denotes the impact parameter, i.e. the distance in the transverse plane to the place where the density is being probed, and J_0 is a cylindrical Bessel Function of order zero [100, 105]. Note that the Dirac FF at $Q^2 = 0$ and the anomalous magnetic moment can be rederived from the transverse charge and magnetization densities

$$\begin{aligned}2\pi \int d\rho \rho \rho_{\text{ch}} &= F_1(0), \\ \pi \int d\rho \rho \rho_{\text{m}} &= \kappa,\end{aligned}\quad (47)$$

either for the nucleon or for each individual flavor. The anomalous magnetization density in the transverse plane [105, 106] is defined as

$$\rho_{\text{m}} = -b \frac{d}{db} \rho_2(b) = b \int_0^\infty \frac{dQ}{2\pi} Q^2 J_1(Qb) F_2(Q^2), \quad (48)$$

where $\rho_2(b)$ is related to the Pauli FF in the same way as $\rho_{\text{ch}}(b)$ to the Dirac FF:

$$\rho_2(b) = \int_0^\infty \frac{dQ}{2\pi} Q J_0(Qb) F_2(Q^2). \quad (49)$$

We first examine the profiles of the transverse charge densities inside an unpolarized nucleon, as shown in Fig. 10. In the left-upper panel of Fig. 10, the transverse charge density inside a proton becomes larger, which indicates that the relativistic effects enhance the density in the center of the proton while lessen the outer part. This can be understood from the results of the Dirac FFs in Fig. 7 and also from Eq.(31). When the relativistic effects are taken into account, the Dirac FFs fall off more slowly than those without these effects. It implies that the size of the proton becomes smaller due to the relativistic effects. Thus, the transverse charge density in the core of the proton is enhanced, which results in its decrease in the outer part, because the density is constrained by the proton charge as shown in Eq.(47). The transverse charge density inside the neutron exhibits a similar feature (see the left-lower panel of Fig. 10). The inset of the left-lower panel designates the quantity $b\rho(b)$, in which we can clearly see that the negative charge is located in the center of the neutron, which is in agreement with that of Ref. [100]. The upper-right and lower-right panels of Fig. 10 illustrate the charge densities in the transverse plane for the proton and the neutron, respectively. Without the polarization of the nucleon, they are distributed in the transverse plane in a spherically symmetric way. In Fig. 11, the transverse magnetization densities inside both the proton and the neutron are drawn. We find similar features like the transverse charge ones, that is, the densities are likely to be squeezed into the center of the nucleon when the relativistic effects are turned on.

The transverse charge and magnetization densities for each flavor are presented in Fig. 12. We find similar behaviors to the case of the transverse charge and magnetization densities inside a proton (see Figs. 10 and 11). However, the relativistic effects are more clearly seen in the transverse charge densities for the up quark than for the down quark. Those for the strange quark show interesting features. While they are found to be positive in the inner region, they become negative as b increases. In Fig. 13, the transverse magnetization densities are depicted for each flavor. Again,

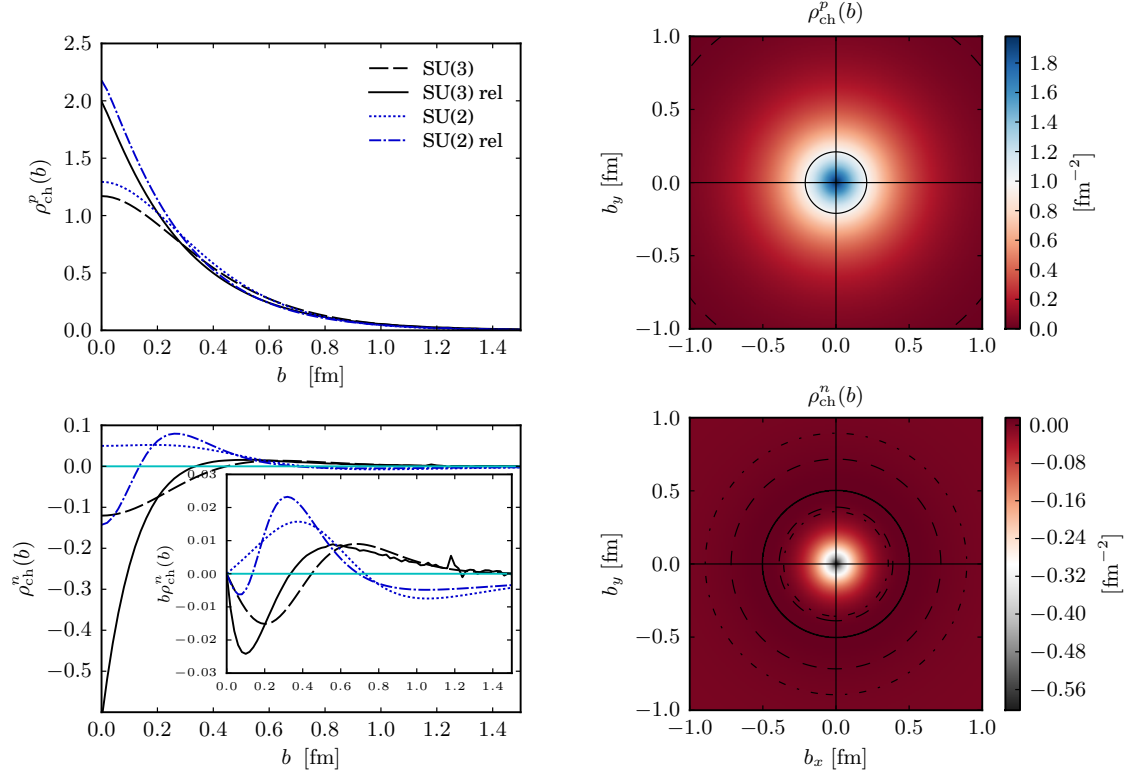


Figure 10. Transverse charge densities inside a proton (upper panel) and a neutron (lower panel). In the upper-left panel, the transverse charge densities inside the proton are depicted as functions of b for each case with the same notation as given in Fig. 1. The upper-right panel illustrates the transverse charge density from the SU(3) model with the relativistic corrections. The contour is drawn at $\rho_p = 0.02$. The inset depicts $b\rho(b)$ for the neutron. For the neutron, the contours are depicted at $\rho_n = 0.005$ (dash-dot), $\rho_n = 0.01$ (dashes) and at maximum positive value (solid).

the relativistic effects in general tend to push the densities towards the center of the nucleon. Note that the down quark inside a nucleon is more magnetized than the up quark but was directed opposite to the up quark, which results in the negative larger value of the anomalous magnetic moment for the down quark than for the up quark (see Eqs.(43, 44)). The transverse magnetization densities are designated in the right panel. They look very different from those for the up and down quarks: In the inner part of the nucleon, the strange quark is negatively magnetized. As b increases, the strange magnetization density turns positive. As a result, the strange anomalous magnetic moment turns out to be small but positive: $\kappa_s = 0.10$ (see Eq.(43)).

When the nucleon is transversely polarized in the xy plane, which can be described by the transverse spin operator of the nucleon $\mathbf{S}_\perp = \cos\phi_S \hat{e}_x + \sin\phi_S \hat{e}_y$, The transverse charge density inside a transversely polarized nucleon is expressed as [101]

$$\rho_T(\mathbf{b}) = \rho_{\text{ch}}(b) - \sin(\phi_b - \phi_S) \frac{1}{2M_N b} \rho_m(b), \quad (50)$$

where $\rho_m(b)$ is given in Eq.(48). The position vector \mathbf{b} from the center of the nucleon in the transverse plane is denoted by $\mathbf{b} = b(\cos\phi_b \hat{e}_x + \sin\phi_b \hat{e}_y)$. The x axis is taken as the polarization direction of the nucleon, i.e. $\phi_S = 0$. In the left panel of Fig. 14, we plot the transverse charge densities inside a transversely polarized proton. It is shown that the charge density for the transversely polarized proton is distorted in the negative y direction. As discussed in Refs. [98, 101], the transverse polarization of the nucleon in the x axis induces the electric dipole moment along the negative y direction, which is a well-known relativistic effect. In the case of the neutron, the situation is even more dramatic. As shown in Fig. 10, the negative charge is located in the center of the neutron, whereas the positive charge is surrounded. However, when the neutron is transversely polarized along the x axis, the negative charge is shifted to the negative y direction but the positive one is moved to the positive y direction. This is due to the fact that the neutron anomalous magnetic moment is negative, which yields an induced electric dipole moment along the positive

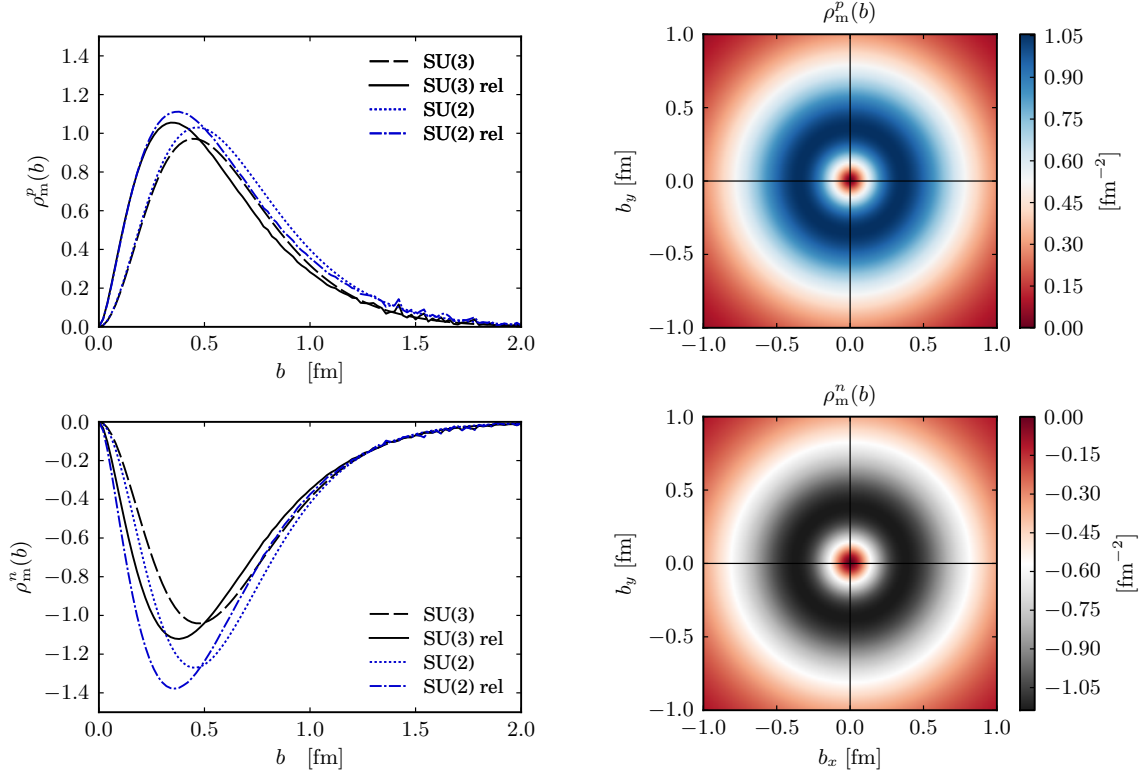


Figure 11. Transverse magnetization densities inside a proton (upper panel) and a neutron (lower panel). In the upper-left panel, the transverse magnetization densities inside the proton are depicted as functions of b for each case with the same notation as given in Fig. 1. The upper-right panel illustrates the transverse magnetization density from the SU(3) model with the relativistic corrections.

y axis, as pointed out by Ref. [101].

It is very instructive to examine the charge densities inside the transversely polarized nucleon for each flavor, since they reveal the inner structure of the nucleon more in detail. Figure 15 illustrates them. The up transverse charge density inside the transversely polarized nucleon is shown to be shifted to the negative direction, while that for the down quark is more distorted upwards. It is natural, since the up and down quarks have positive and negative charges, respectively. However, it is remarkable to see that the down quark is influenced more strongly due to the transverse polarization of the nucleon. The charge density inside the transversely polarized nucleon for the strange quark is even more interesting. As discussed previously, the strange anomalous magnetic moment is $\kappa_s = +0.10$, which would induce the negative electric dipole moment along the negative b_y . However, situation turns out to be more complicated. As shown in the right panel of Fig. 15, the strange charge density is shifted to the positive b_y and becomes even negative in the uppermost region. In order to understand this surprising result, we need to reexamine the transverse magnetization density for the strange quark, which has been presented in Fig. 13. The strange magnetization density is negative in the inner part of the nucleon, it turns positive around $b \approx 0.7$ fm. Thus, the electric dipole moment is induced along the positive y direction, while it becomes negative, as drawn in the right panel of Fig. 15.

V. SUMMARY AND CONCLUSION

In the present work, we aimed at investigating the electromagnetic properties of the nucleon, based on the SU(2) and SU(3) chiral quark-soliton model with a symmetry-preserving quantization employed. We considered the rotational $1/N_c$ corrections and the first-order m_s corrections. Though the model is valid in lower energy regions ($Q^2 \lesssim 1 \text{ GeV}^2$), we took into account the relativistic boost effects on the electromagnetic form factors of the nucleon so that we can describe the form factors for higher Q^2 .

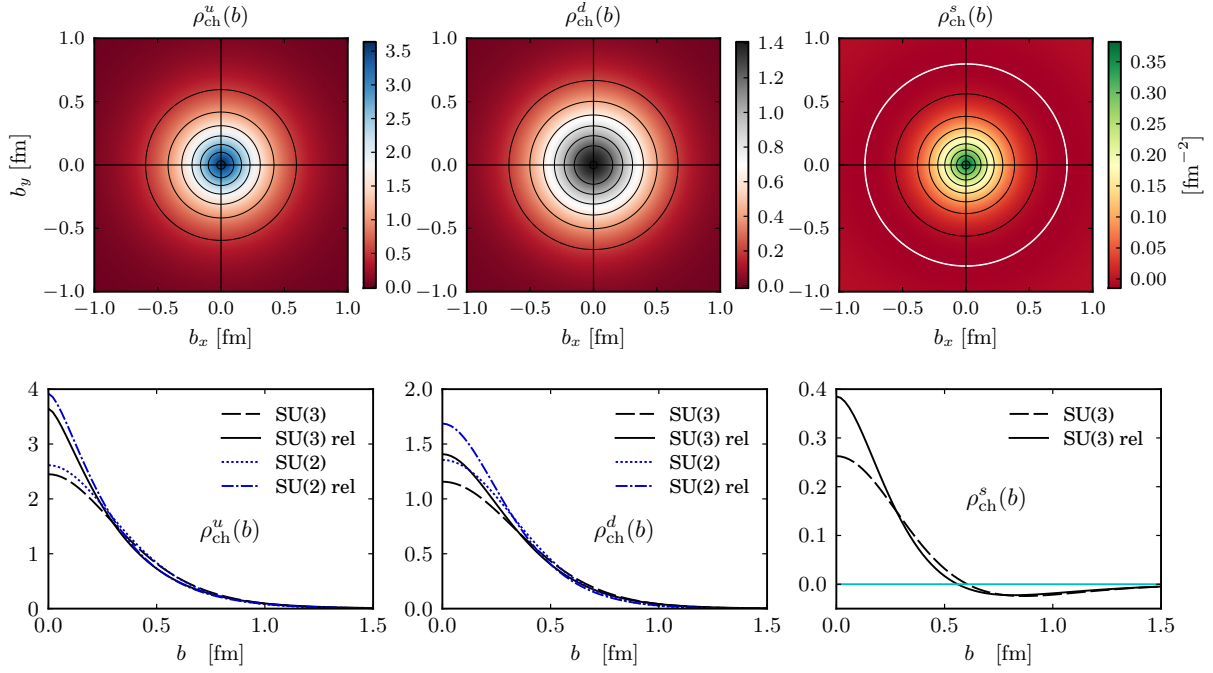


Figure 12. Flavor-decomposed transverse charge densities inside a proton. The contours are drawn according to the color bars, which have different sizes. In the case of the strange charge density, the white contour corresponds to the minimum value of the density, which is negative.

We first presented the results of the model for the nucleon electromagnetic form factors normalized by the dipole form factor. We found that the proton electric form factor with relativistic corrections describes the experimental data very well, whereas the proton magnetic form factor is slightly overestimated. The neutron electric form factor with the relativistic effects is quite underestimated in comparison with the data, but that from the SU(2) model looks overestimated. Since the neutron form factor is known to be very sensitive to the soliton tail, one possibly understands why the SU(3) results are rather different from those in SU(2). We then examined the ratios of the nucleon electric and magnetic form factors. It was found that the SU(3) results explained the general tendency of the experimental data for the proton but those of SU(2) turned out to be overestimated, as Q^2 increased. The results for the ratio of the neutron electric and magnetic form factors were compared with the data. In this case, the SU(2) model successfully describes the experimental data, while the SU(3) results are smaller than the data. A possible explanation about this discrepancy between the SU(2) and SU(3) results was given by the sensitivity of the neutron electric form factor to the soliton tail. We also studied the flavor decomposition of the nucleon electromagnetic form factors. We observed that the up magnetic and down electric form factors normalized by the dipole parametrization were well reproduced, with the relativistic effects taken into account. When we turned off them, the results were shown to deviate from the data as Q^2 increased. The up electric form factor obtained from the SU(3) model with the relativistic effects was yielded to be qualitatively similar to the data, whereas the down magnetic form factors departed from them. The strange electromagnetic form factors normalized by the dipole one were predicted. In general, the strange form factors with the relativistic effects turned out to be larger than those without them.

The Dirac and Pauli form factors were predicted to be asymptotically proportional to $1/Q^4$ and $1/Q^6$ respectively in perturbative QCD. Thus, $Q^4 F_1^p(Q^2)$ and $Q^6 F_2(Q^2)$ were measured experimentally to examine their Q^2 dependence. We found that the present SU(2) model explained well $Q^4 F_1(Q^2)$ for both the proton and the neutron. The results for $Q^6 F_2^{p,n}(Q^2)$ described the experimental data very well below $Q^2 \lesssim 1 \text{ GeV}^2$. As Q^2 increases, the results turn out to be overestimated. The ratio $Q^2 \kappa^N F_2^N / F_1^N$ were also computed and their results showed similar tendencies in comparison with the data. Since the experimental data clearly reveal different Q^2 dependencies of $F_{1,2}^u$ and $F_{1,2}^d$, we found that the results for the up Dirac and Pauli form factors were in remarkable agreement with the data, while the down form factors were overestimated in magnitude. The strange Dirac and Pauli form factors were predicted. The ratios of the Pauli form factors to the Dirac were qualitatively explained.

Having performed the two-dimensional Fourier transform of the nucleon electromagnetic form factors, we were able to produce the charge densities in the transverse plane inside a proton. We found that the relativistic effects enhanced the density in the center of the proton while diminished it as b increased. A similar tendency was observed

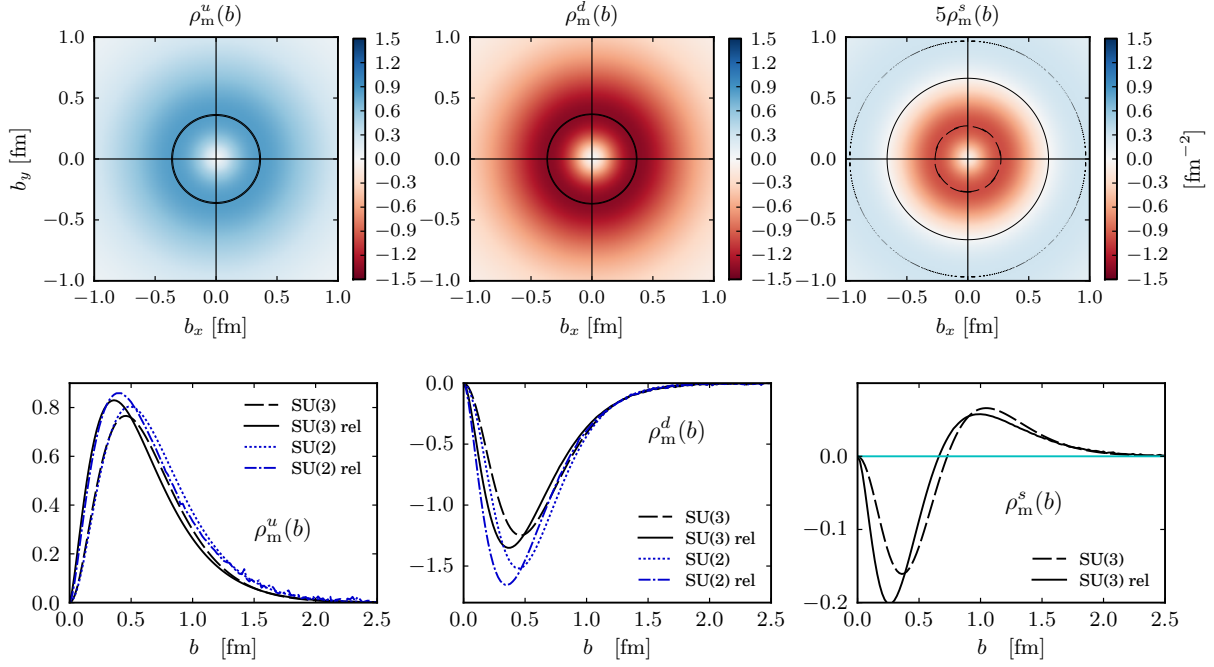


Figure 13. Flavor-decomposed transverse anomalous magnetic densities inside a proton. For the u quark the contour represents the maximum value of the density, while for the d quark it corresponds to the minimum of the density. In the case of the s quark, the dashed (inner) contour corresponds to the minimum of the density, the solid (middle) contour to the null density, and the dotted (outer) contour to the maximum of the density. The strange quark density is scaled by 5 in order to increase its readability.

in the transverse charge density inside a neutron. However, the negative charge was located in the center of the neutron while the positive one was distributed in outer part. The results of the transverse magnetization revealed similar features like the transverse charge ones: the densities were squeezed into the center of the nucleon when the relativistic effects were considered. We then decomposed the transverse charge and magnetization densities for each flavor. It was found that the flavor-decomposed transverse charge densities exhibited similar features to the case of the transverse charge and magnetization densities inside a proton. The relativistic effects were more clearly observed in the transverse charge densities for the up quark than for the down quark. Those for the strange quark were shown to be positive in the inner region and then become negative as b increases. On the other hand, the strange quark was found to be negatively magnetized in the inner part of the nucleon. As b increased, the magnetization of the strange quark changed to positive values. As a result, the strange anomalous magnetic moment turns out to be small but positive: $\kappa_s = +0.10$.

When the proton was polarized along the positive x direction, its transverse charge density was shifted to the negative y direction, which indicated that the electric dipole moment was induced along the negative y direction. It is just a well-known relativistic effect. In the case of the neutron polarized along the x axis, the negative charge was moved to the negative y direction but the positive one was forced to the positive y axis. It implies that the neutron anomalous magnetic moment is negative, which induces an electric dipole moment along the positive y axis. We also decomposed the transverse charge densities inside the polarized nucleon for each flavor: the up transverse charge density for the nucleon transversely polarized along the positive x axis was found to be shifted to the negative direction, while that for the down quark was more distorted upwards. Since the up and down quarks have positive and negative charges, respectively, one can easily understand these features. However, the down quark was found to be affected more strongly due to the transverse polarization of the nucleon. The strange charge density inside the transversely polarized nucleon was shifted to the positive b_y and turned out to be negative in the uppermost region. This unexpected behavior of the strange charge density for the transversely polarized nucleon was explained in terms of the strange magnetization density.

Since the transverse charge densities inside unpolarized and polarized nucleons pave the novel way for understanding the internal structure of the nucleon, it is interesting to investigate them for other baryons such as the Δ isobar and hyperons. The transverse charge densities are directly connected to the generalized parton distributions of which the integrations over parton momentum fractions yield form factors and consequently the spatial distribution of partons

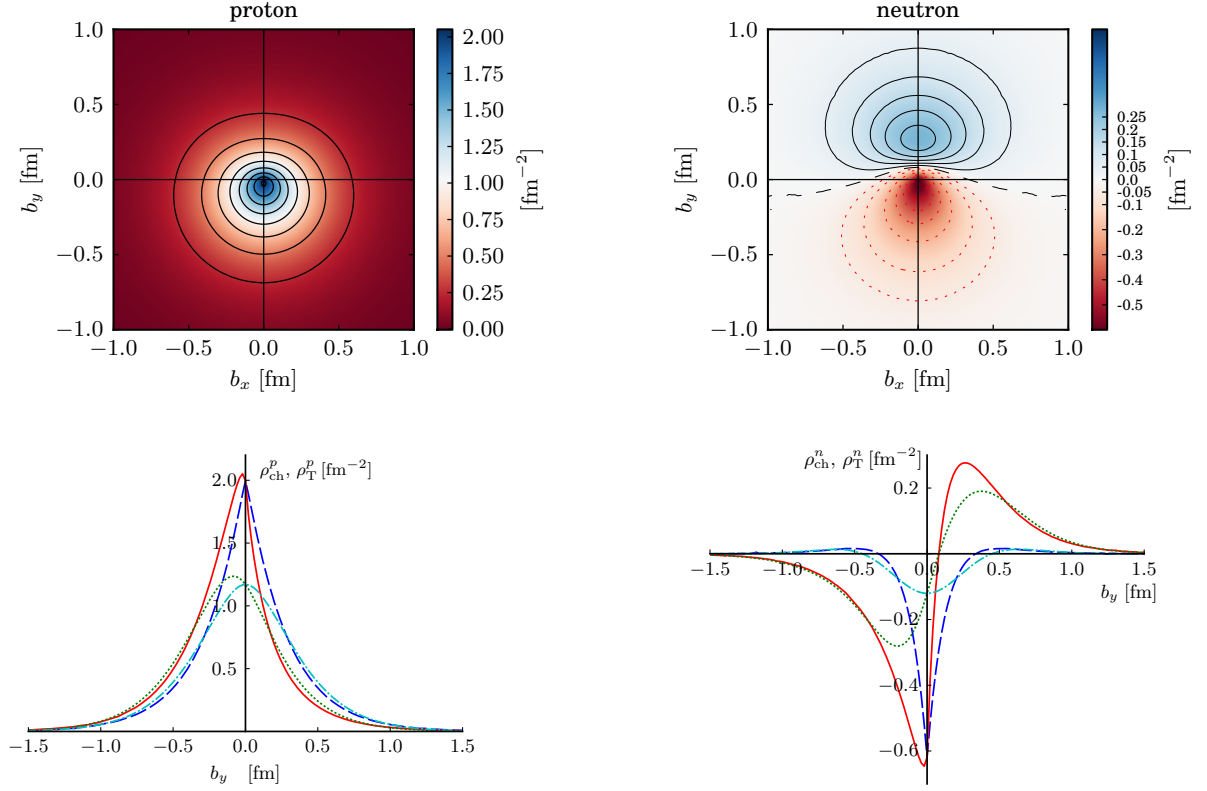


Figure 14. Transverse charge densities inside a polarized nucleon. The upper panel shows the transverse charge densities inside a proton polarized along the x axis (left panel) and a neutron (right panel) in the relativistic SU(3) case. The lower panel depicts the corresponding transverse charge densities in the y axis: The solid curve corresponds to the relativistic results, shown in the upper panel, and the dashed curve to the unpolarized case, for comparison. The dotted and dash-dotted curves represent the SU(3) results for the transverse densities in the rest frame, polarized and unpolarized, respectively.

in the transverse plane. Moreover, the transverse charge densities for transition form factors provide a new aspect of understanding the inner structure of the baryons. For example, as Ref. [101] already studied, they exhibit explicitly multipole structures of the transitions in the transverse plane. Thus, it is of great importance to examine the transverse charge densities for other baryons and for their transitions. Corresponding investigations are under way.

ACKNOWLEDGMENTS

The work of H.Ch.K. was supported by Basic Science Research Program through the National Research Foundation of Korea funded by the Ministry of Education, Science and Technology (Grant Number: 2012R1A1A2001083).

-
- [1] M. K. Jones *et al.* [Jefferson Lab Hall A Collaboration], Phys. Rev. Lett. **84**, 1398 (2000) [nucl-ex/9910005].
 - [2] O. Gayou *et al.* [Jefferson Lab Hall A Collaboration], Phys. Rev. C **64**, 038202 (2001).
 - [3] O. Gayou *et al.* [Jefferson Lab Hall A Collaboration], Phys. Rev. Lett. **88**, 092301 (2002) [nucl-ex/0111010].
 - [4] V. Punjabi *et al.* [Jefferson Lab Hall A Collaboration], Phys. Rev. C **71**, 055202 (2005) [Erratum-ibid. C **71**, 069902 (2005)] [nucl-ex/0501018].
 - [5] A. J. R. Puckett, E. J. Brash, M. K. Jones, W. Luo, M. Meiziane, L. Pentchev, C. F. Perdrisat and V. Punjabi *et al.*, Phys. Rev. Lett. **104**, 242301 (2010) [arXiv:1005.3419 [nucl-ex]].
 - [6] J. C. Bernauer *et al.* [A1 Collaboration], Phys. Rev. Lett. **105**, 242001 (2010) [arXiv:1007.5076 [nucl-ex]].
 - [7] G. Ron *et al.* [Jefferson Lab Hall A Collaboration], Phys. Rev. C **84**, 055204 (2011) [arXiv:1103.5784 [nucl-ex]].

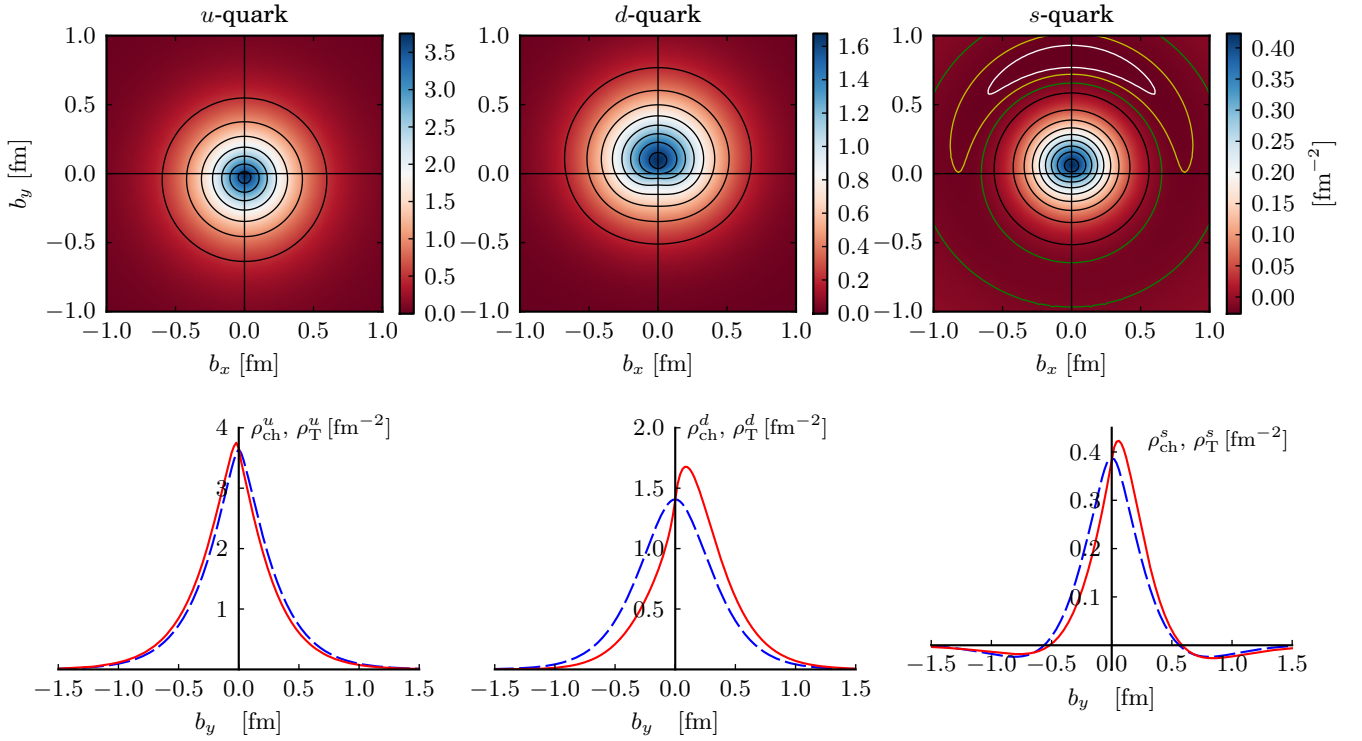


Figure 15. Flavor transverse charge densities. The upper panel shows the flavor transverse charge densities inside a proton polarized along the x -axis. For the strange quark the charge density becomes negative in the positive b_y . The values for the outmost contours are given as -0.015 (green), -0.0225 (yellow) and -0.0255 (white). The lower panel shows the corresponding transverse flavor densities with b_x fixed for the polarized (solid curve) case and the unpolarized one (dashed curve), respectively.

- [8] X. Zhan, K. Allada, D. S. Armstrong, J. Arrington, W. Bertozzi, W. Boeglin, J. -P. Chen and K. Chirapatpimol *et al.*, Phys. Lett. B **705**, 59 (2011) [arXiv:1102.0318 [nucl-ex]].
- [9] M. N. Rosenbluth, Phys. Rev. **79**, 615 (1950).
- [10] C. E. Hyde-Wright and K. de Jager, Ann. Rev. Nucl. Part. Sci. **54**, 217 (2004) [nucl-ex/0507001].
- [11] J. Arrington, C. D. Roberts and J. M. Zanotti, J. Phys. G **34**, S23 (2007) [nucl-th/0611050].
- [12] C. F. Perdrisat, V. Punjabi and M. Vanderhaeghen, Prog. Part. Nucl. Phys. **59**, 694 (2007) [hep-ph/0612014].
- [13] M. Vanderhaeghen and T. Walcher, arXiv:1008.4225 [hep-ph].
- [14] J. Arrington, K. de Jager and C. F. Perdrisat, J. Phys. Conf. Ser. **299**, 012002 (2011) [arXiv:1102.2463 [nucl-ex]].
- [15] P. A. M. Guichon and M. Vanderhaeghen, Phys. Rev. Lett. **91**, 142303 (2003) [hep-ph/0306007].
- [16] P. G. Blunden, W. Melnitchouk and J. A. Tjon, Phys. Rev. Lett. **91**, 142304 (2003) [nucl-th/0306076].
- [17] J. Arrington, Phys. Rev. C **71**, 015202 (2005) [hep-ph/0408261].
- [18] J. Arrington, W. Melnitchouk and J. A. Tjon, Phys. Rev. C **76**, 035205 (2007) [arXiv:0707.1861 [nucl-ex]].
- [19] C. E. Carlson and M. Vanderhaeghen, Ann. Rev. Nucl. Part. Sci. **57**, 171 (2007) [hep-ph/0701272 [HEP-PH]].
- [20] J. Arrington, P. G. Blunden and W. Melnitchouk, Prog. Part. Nucl. Phys. **66**, 782 (2011) [arXiv:1105.0951 [nucl-th]].
- [21] S. J. Brodsky and G. R. Farrar, Phys. Rev. D **11**, 1309 (1975).
- [22] B. Aubert *et al.* [BABAR Collaboration], Phys. Rev. D **80**, 052002 (2009) [arXiv:0905.4778 [hep-ex]].
- [23] S. Uehara *et al.* [Belle Collaboration], Phys. Rev. D **86**, 092007 (2012) [arXiv:1205.3249 [hep-ex]].
- [24] M. Ostrick, C. Herberg, H. G. Andresen, J. R. M. Annand, K. Aulenbacher, J. Becker, P. Drescher and D. Eyl *et al.*, Phys. Rev. Lett. **83**, 276 (1999).
- [25] I. Passchier, R. Alarcon, T. S. Bauer, D. Boersma, J. F. J. van den Brand, L. D. van Buuren, H. J. Bulten and M. Ferro-Luzzi *et al.*, Phys. Rev. Lett. **82**, 4988 (1999) [nucl-ex/9907012].
- [26] D. Rohe *et al.* [A1 Collaboration], Phys. Rev. Lett. **83**, 4257 (1999).
- [27] H. Zhu *et al.* [Jefferson Lab E93-026 Collaboration], Phys. Rev. Lett. **87**, 081801 (2001) [nucl-ex/0105001].
- [28] J. Bermuth, P. Merle, C. Carasco, D. Baumann, D. Bohm, D. Bosnar, M. Ding and M. O. Distler *et al.*, Phys. Lett. B **564**, 199 (2003) [nucl-ex/0303015].
- [29] G. Warren *et al.* [Jefferson Lab E93-026 Collaboration], Phys. Rev. Lett. **92**, 042301 (2004) [nucl-ex/0308021].
- [30] D. I. Glazier *et al.* [A1 Collaboration], Eur. Phys. J. A **24**, 101 (2005) [nucl-ex/0410026].
- [31] B. Plaster *et al.* [Jefferson Lab E93-038 Collaboration], Phys. Rev. C **73**, 025205 (2006) [nucl-ex/0511025].
- [32] E. Geis *et al.* [BLAST Collaboration], Phys. Rev. Lett. **101**, 042501 (2008) [arXiv:0803.3827 [nucl-ex]].

- [33] J. Lachniet *et al.* [CLAS Collaboration], Phys. Rev. Lett. **102**, 192001 (2009) [arXiv:0811.1716 [nucl-ex]].
- [34] S. Riordan, S. Abrahamyan, B. Craver, A. Kelleher, A. Kolarkar, J. Miller, G. D. Cates and N. Liyanage *et al.*, Phys. Rev. Lett. **105**, 262302 (2010) [arXiv:1008.1738 [nucl-ex]].
- [35] G. D. Cates, C. W. de Jager, S. Riordan and B. Wojtsekhowski, Phys. Rev. Lett. **106**, 252003 (2011) [arXiv:1103.1808 [nucl-ex]].
- [36] I. A. Qattan and J. Arrington, Phys. Rev. C **86**, 065210 (2012) [arXiv:1209.0683 [nucl-ex]].
- [37] Supplemental Material from [36] at <http://link.aps.org/supplemental/10.1103/PhysRevC.86.065210>
- [38] G. Eichmann, Phys. Rev. D **84**, 014014 (2011) [arXiv:1104.4505 [hep-ph]].
- [39] M. Rohrmoser, K. -S. Choi and W. Plessas, arXiv:1110.3665 [hep-ph].
- [40] I. C. Cloet and G. A. Miller, Phys. Rev. C **86**, 015208 (2012) [arXiv:1204.4422 [nucl-th]].
- [41] J. O. Gonzalez-Hernandez, S. Liuti, G. R. Goldstein and K. Kathuria, arXiv:1206.1876 [hep-ph].
- [42] D. Diakonov, V. Y. Petrov and P. V. Pobylitsa, Nucl. Phys. B **306**, 809 (1988).
- [43] M. Wakamatsu and H. Yoshiki, Nucl. Phys. A **524**, 561 (1991).
- [44] D. Diakonov, In *Peniscola 1997, Advanced school on non-perturbative quantum field physics* 1-55 [hep-ph/9802298].
- [45] K. Goeke, A.Z. Gorski, F. Gruemmer, T. Meissner, H. Reinhardt and R. Wunsch, Phys. Lett. B **256**, 321 (1991).
- [46] A. Blotz, K. Goeke, N. W. Park, D. Diakonov, V. Petrov and P. V. Pobylitsa, Phys. Lett. B **287**, 29 (1992).
- [47] A. Blotz, D. Diakonov, K. Goeke, N. W. Park, V. Petrov and P. V. Pobylitsa, Nucl. Phys. A **555**, 765 (1993).
- [48] H. -Ch. Kim, A. Blotz, M. V. Polyakov and K. Goeke, Phys. Rev. D **53**, 4013 (1996) [hep-ph/9504363].
- [49] H. -Ch. Kim, A. Blotz, C. Schneider and K. Goeke, Nucl. Phys. A **596**, 415 (1996) [hep-ph/9508299].
- [50] A. Silva, H. -Ch. Kim and K. Goeke, Phys. Rev. D **65**, 014016 (2002) [Erratum-ibid. D **66**, 039902 (2002)] [hep-ph/0107185].
- [51] A. Silva, H. -Ch. Kim and K. Goeke, Eur. Phys. J. A **22**, 481 (2004) [hep-ph/0210189].
- [52] A. Silva, H. -Ch. Kim, D. Urbano and K. Goeke, Phys. Rev. D **72**, 094011 (2005) [hep-ph/0509281].
- [53] A. Silva, H. -Ch. Kim, D. Urbano and K. Goeke, Phys. Rev. D **74**, 054011 (2006) [hep-ph/0601239].
- [54] K. Goeke, H. -Ch. Kim, A. Silva and D. Urbano, Eur. Phys. J. A **32**, 393 (2007) [hep-ph/0608262].
- [55] K. Goeke, J. Grabis, J. Ossmann, M. V. Polyakov, P. Schweitzer, A. Silva and D. Urbano, Phys. Rev. D **75**, 094021 (2007) [hep-ph/0702030].
- [56] H. -Ch. Kim, M. Praszalowicz and K. Goeke, Phys. Rev. D **57**, 2859 (1998) [hep-ph/9706531].
- [57] G. -S. Yang, H. -C. Kim, M. Praszalowicz and K. Goeke, Phys. Rev. D **70**, 114002 (2004) [hep-ph/0410042].
- [58] H. -Ch. Kim, M. Polyakov, M. Praszalowicz, G. -S. Yang and K. Goeke, Phys. Rev. D **71**, 094023 (2005) [hep-ph/0503237].
- [59] H. -Ch. Kim, M. V. Polyakov, M. Praszalowicz and K. Goeke, Phys. Rev. D **57**, 299 (1998) [hep-ph/9709221].
- [60] H. -Ch. Kim, M. Praszalowicz and K. Goeke, Phys. Rev. D **61**, 114006 (2000) [hep-ph/9910282].
- [61] T. Ledwig, A. Silva, H. -Ch. Kim and K. Goeke, JHEP **0807**, 132 (2008) [arXiv:0806.4072 [hep-ph]].
- [62] T. Watabe, C. V. Christov and K. Goeke, Phys. Lett. B **349**, 197 (1995) [hep-ph/9502244].
- [63] A. Silva, D. Urbano, T. Watabe, M. Fiolhais and K. Goeke, Nucl. Phys. A **675**, 637 (2000) [hep-ph/9905326].
- [64] T. Ledwig, A. Silva and M. Vanderhaeghen, Phys. Rev. D **79**, 094025 (2009) [arXiv:0811.3086 [hep-ph]].
- [65] H. -Ch. Kim, M. V. Polyakov and K. Goeke, Phys. Rev. D **53**, 4715 (1996) [hep-ph/9509283].
- [66] H. -Ch. Kim, M. V. Polyakov and K. Goeke, Phys. Lett. B **387**, 577 (1996) [hep-ph/9604442].
- [67] P. Schweitzer, D. Urbano, M. V. Polyakov, C. Weiss, P. V. Pobylitsa and K. Goeke, Phys. Rev. D **64**, 034013 (2001) [hep-ph/0101300].
- [68] T. Ledwig, A. Silva and H. -Ch. Kim, Phys. Rev. D **82**, 034022 (2010) [arXiv:1004.3612 [hep-ph]].
- [69] T. Ledwig, A. Silva and H. -Ch. Kim, Phys. Rev. D **82**, 054014 (2010) [arXiv:1007.1355 [hep-ph]].
- [70] T. Ledwig and H. -Ch. Kim, Phys. Rev. D **85**, 034041 (2012) [arXiv:1107.4952 [hep-ph]].
- [71] B. Dressler, K. Goeke, M. V. Polyakov and C. Weiss, Eur. Phys. J. C **14**, 147 (2000) [hep-ph/9909541].
- [72] B. Dressler, K. Goeke, M. V. Polyakov, P. Schweitzer, M. Strikman and C. Weiss, Eur. Phys. J. C **18**, 719 (2001) [hep-ph/9910464].
- [73] K. Goeke, P. V. Pobylitsa, M. V. Polyakov, P. Schweitzer and D. Urbano, Acta Phys. Polon. B **32**, 1201 (2001) [hep-ph/0001272].
- [74] J. Ossmann, M. V. Polyakov, P. Schweitzer, D. Urbano and K. Goeke, Phys. Rev. D **71**, 034011 (2005) [hep-ph/0411172].
- [75] M. Wakamatsu and Y. Nakakoji, hep-ph/0605279.
- [76] M. Wakamatsu, Phys. Rev. D **72**, 074006 (2005).
- [77] M. Wakamatsu, Phys. Rev. D **67**, 034006 (2003).
- [78] M. Wakamatsu, Phys. Lett. B **487**, 118 (2000).
- [79] R. Alkofer, H. Reinhardt and H. Weigel, Phys. Rept. **265**, 139 (1996).
- [80] C. V. Christov, A. Blotz, H. -Ch. Kim, P. Pobylitsa, T. Watabe, T. Meissner, E. Ruiz Arriola and K. Goeke, Prog. Part. Nucl. Phys. **37**, 91 (1996) [hep-ph/9604441].
- [81] H. Weigel, Lect. Notes Phys. **743**, 1 (2008).
- [82] K. A. Aniol *et al.* [HAPPEX Collaboration], Phys. Lett. B **509**, 211 (2001) [nucl-ex/0006002].
- [83] F. E. Maas *et al.* [A4 Collaboration], Phys. Rev. Lett. **93**, 022002 (2004) [nucl-ex/0401019].
- [84] F. E. Maas, K. Aulenbacher, S. Baunack, L. Capozza, J. Diefenbach, B. Glaser, T. Hammel and D. von Harrach *et al.*, Phys. Rev. Lett. **94**, 152001 (2005) [nucl-ex/0412030].
- [85] D. S. Armstrong *et al.* [G0 Collaboration], Phys. Rev. Lett. **95**, 092001 (2005) [nucl-ex/0506021].
- [86] A. Acha *et al.* [HAPPEX Collaboration], Phys. Rev. Lett. **98**, 032301 (2007) [nucl-ex/0609002].

- [87] S. Baunack, K. Aulenbacher, D. Balaguer Rios, L. Capozza, J. Diefenbach, B. Glaser, D. von Harrach and Y. Imai *et al.*, Phys. Rev. Lett. **102**, 151803 (2009) [arXiv:0903.2733 [nucl-ex]].
- [88] D. Androic *et al.* [G0 Collaboration], Phys. Rev. Lett. **104**, 012001 (2010) [arXiv:0909.5107 [nucl-ex]].
- [89] S. F. Pate and J. P. Schaub, J. Phys. Conf. Ser. **295**, 012037 (2011) [arXiv:1012.2991 [hep-ex]].
- [90] Z. Ahmed *et al.* [HAPPEX Collaboration], Phys. Rev. Lett. **108**, 102001 (2012) [arXiv:1107.0913 [nucl-ex]].
- [91] D. S. Armstrong and R. D. McKeown, Ann. Rev. Nucl. Part. Sci. **62**, 337 (2012) [arXiv:1207.5238 [nucl-ex]].
- [92] M. Praszalowicz, T. Watabe and K. Goeke, Nucl. Phys. A **647**, 49 (1999) [hep-ph/9806431].
- [93] X. -D. Ji, J. Phys. G **24**, 1181 (1998) [hep-ph/9807358].
- [94] K. Goeke, M. V. Polyakov and M. Vanderhaeghen, Prog. Part. Nucl. Phys. **47**, 401 (2001) [hep-ph/0106012].
- [95] M. Diehl, Phys. Rept. **388**, 41 (2003) [hep-ph/0307382].
- [96] A. V. Belitsky and A. V. Radyushkin, Phys. Rept. **418**, 1 (2005) [hep-ph/0504030].
- [97] M. Burkardt, Phys. Rev. **D62** (2000) 071503. [hep-ph/0005108].
- [98] M. Burkardt, Int. J. Mod. Phys. **A18** (2003) 173-208. [arXiv:hep-ph/0207047 [hep-ph]].
- [99] M. Diehl and P. Hagler, Eur. Phys. J. **C44** (2005) 87.
- [100] G. A. Miller, Phys. Rev. Lett. **99**, 112001 (2007) [arXiv:0705.2409 [nucl-th]].
- [101] C. E. Carlson and M. Vanderhaeghen, Phys. Rev. Lett. **100**, 032004 (2008) [arXiv:0710.0835 [hep-ph]].
- [102] M. Gockeler *et al.* [QCDSF Collaboration and UKQCD Collaboration], Phys. Rev. Lett. **98** (2007) 222001.
- [103] J. J. Kelly, Phys. Rev. C **66**, 065203 (2002) [hep-ph/0204239].
- [104] A. N. Mitra and I. Kumari, Phys. Rev. D **15**, 261 (1977).
- [105] G. A. Miller, Ann. Rev. Nucl. Part. Sci. **60**, 1 (2010) [arXiv:1002.0355 [nucl-th]].
- [106] S. Venkat, J. Arrington, G. A. Miller and X. Zhan, Phys. Rev. C **83**, 015203 (2011) [arXiv:1010.3629 [nucl-th]].
- [107] B. D. Milbrath *et al.* [Bates FPP Collaboration], Phys. Rev. Lett. **80** (1998) 452 [Erratum-ibid. **82** (1999) 2221] [nucl-ex/9712006].
- [108] T. Pospischil *et al.* [A1 Collaboration], Eur. Phys. J. A **12**, 125 (2001).
- [109] G. MacLachlan, A. Aghalarian, A. Ahmidouch, B. D. Anderson, R. Asaturian, O. Baker, A. R. Baldwin and D. Barkhuff *et al.*, Nucl. Phys. A **764**, 261 (2006).
- [110] M. Paolone, S. P. Malace, S. Strauch, I. Albayrak, J. Arrington, B. L. Berman, E. J. Brash and W. J. Briscoe *et al.*, Phys. Rev. Lett. **105**, 072001 (2010) [arXiv:1002.2188 [nucl-ex]].
- [111] A. J. R. Puckett, E. J. Brash, O. Gayou, M. K. Jones, L. Pentchev, C. F. Perdrisat, V. Punjabi and K. A. Aniol *et al.*, Phys. Rev. C **85**, 045203 (2012) [arXiv:1102.5737 [nucl-ex]].
- [112] M. K. Jones *et al.* [Resonance Spin Structure Collaboration], Phys. Rev. C **74**, 035201 (2006) [nucl-ex/0606015].
- [113] C. B. Crawford, A. Sindile, T. Akdogan, R. Alarcon, W. Bertozzi, E. Booth, T. Botto and J. Calarco *et al.*, Phys. Rev. Lett. **98**, 052301 (2007) [nucl-ex/0609007].
- [114] C. Herberg, M. Ostrick, H. G. Andresen, J. R. M. Annand, K. Aulenbacher, J. Becker, P. Drescher and D. Eyl *et al.*, Eur. Phys. J. A **5**, 131 (1999).
- [115] F. J. Ernst, R. G. Sachs, K. C. Wali and , Phys. Rev. **119**, 1105 (1960).
- [116] R. G. Sachs, Phys. Rev. **126**, 2256 (1962).
- [117] C. V. Christov, A. Z. Gorski, K. Goeke, and P. V. Pobylitsa, Nucl. Phys. A **592**, 513 (1995) [hep-ph/9507256].
- [118] R. G. Arnold, C. E. Carlson, and F. Gross, Phys. Rev. C **23**, 363 (1981).
- [119] A. L. Licht, and A. Pagnamenta, Phys. Rev. D **2**, 1156 (1970).
- [120] G. Holzwarth, Z. Phys. A **356**, 339 (1996) [hep-ph/9606336].
- [121] X. -D. Ji, Phys. Lett. B **254**, 456 (1991).